NACA

RESEARCH MEMORANDUM

A PRESSURE-DISTRIBUTION INVESTIGATION OF A SUPERSONIC-AIRCRAFT FUSELAGE AND CALIBRATION OF THE MACH NUMBER 1.40 NOZZLE OF THE LANGLEY 4- BY 4-FOOT SUPERSONIC TUNNEL

By Lowell E. Hasel and Archibald R. Sinclair

Langley Aeronautical Laboratory
Langley Air Force Base, Va.

NATIONAL ADVISORY COMMITTEE
FOR AERONAUTICS

WASHINGTON

April 7, 1950
Declassified May 29, 1959

NATIONAL ADVISORY COMMITTEE FOR AERONAUTICS

RESEARCH MEMORANDUM

A PRESSURE-DISTRIBUTION INVESTIGATION OF A SUPERSONIC-AIRCRAFT FUSELAGE AND CALIBRATION OF THE MACH NUMBER 1.40 NOZZLE OF THE LANGLEY 4- BY 4-FOOT SUPERSONIC TUNNEL

By Lowell E. Hasel and Archibald R. Sinclair

SUMMARY

Pressure-distribution tests of a supersonic-aircraft fuselage with and without canopies (body of revolution without canopies) have been conducted in the Langley 4- by 4-foot supersonic tunnel at a Mach number of 1.40 and a Reynolds number of 2.7×10^6. These data, which were obtained upon completion of a series of calibration tests of the nozzle at a Mach number of 1.40, are compared with linear and nonlinear theoretical results. The results of the calibration tests indicated that the flow in the test section in the vicinity of the model is sufficiently uniform to allow reliable data to be obtained.

For the fuselage without canopies (body of revolution) very good agreement between the experimental results and the rigorous linear theory was obtained through the entire angle-of-attack range (10° maximum) over most of the body. A comparison of the rigorous and incomplete linear theories indicates the importance of the radial-perturbation-velocity term which the latter theory neglects in determining the pressure coefficient. It is also pointed out that nonlinear solutions for the pressures on arbitrary bodies of revolution which have the same form of solution as the incomplete linear theory appear to be inadequate in the same respects as the incomplete linear solutions.

INTRODUCTION

An experimental investigation has been in progress in the Langley 4- by 4-foot supersonic tunnel to determine the aerodynamic characteristics of a large model of a sweptback-wing airplane. The test model was selected to represent a supersonic-aircraft configuration in order that fundamental data having immediate practical interest would be obtained. As a part of this investigation, a relatively detailed study of the pressure distribution over the fuselage of this airplane has been made. The first series of these tests has been made at a Mach number of 1.59 and the results have been presented in reference 1.

This paper presents the results of a similar investigation at a Mach number of 1.40 and a Reynolds number of 2.7×10^6, and may be regarded as an extension at another Mach number of the tests presented and discussed in reference 1. The experimental pressure distributions obtained on the fuselage with and without canopies are presented. In addition, the results obtained from the fuselage without canopies are compared with linear and nonlinear theoretical results. Calibration data of the test-section flow at Mach number 1.40 have also been included to serve as a reference for future reports.

SYMBOLS

Free-stream conditions:

ρ	mass density of air
V	airspeed
a	speed of sound in air
M	Mach number (V/a)
q	dynamic pressure $\left(\frac{1}{2}\rho V^2\right)$
p	static pressure

Local model conditions:

u	axial perturbation velocity
v	radial perturbation velocity

Fuselage geometry:

α	angle of attack of fuselage center line measured in the plane of symmetry of the airplane
ϕ	fuselage polar angle measured in a plane perpendicular to the longitudinal axis, degrees (0° at bottom of fuselage, see fig. 8)

Air-stream geometry:

θ_H angle between tunnel center line and flow direction measured in a horizontal plane, positive to right when viewed looking upstream (see fig. 1)

θ_V angle between tunnel center line and flow direction measured in a vertical plane, positive for upflow (see fig. 1)

Pressure data:

p_l local static pressure

P pressure coefficient $\left(\frac{p_l - p}{q}\right)$

LANGLEY 4- BY 4-FOOT SUPERSONIC TUNNEL

General Description

The Langley 4- by 4-foot supersonic tunnel is a closed-throat, single-return wind tunnel (see fig. 1, reference 1) driven by an axial-flow compressor. The tunnel has been designed for a nominal Mach number range from 1.2 to 2.2 and is temporarily powered by a 6000-horsepower electric-drive system. With the present power, the stagnation pressure is limited to approximately 0.3 atmosphere. The tunnel has a rectangular nozzle and test section consisting of two fixed parallel side walls and two horizontal flexible nozzle walls. The side walls and nozzle walls are 25 feet long and are continuous from a point 66 inches upstream of the throat to the end of the test section (fig. 1). For the Mach number 1.40 nozzle, the test section has a width of 4.5 feet, a height of 4.4 feet, and a length of uniform-flow region along the wall of approximately 7 feet.

The supersonic nozzle and test section are formed by deflecting the horizontal flexible walls against a series of fixed interchangeable templates which have been designed to give a wall shape producing uniform flow in the test section. For this series of tests, temporary mild-steel nozzle plates were used in place of the permanent set of machined and polished stainless-steel plates. These temporary plates contain some small periodic waves.

Aerodynamic Design

The flexible-wall section of the tunnel extends from station 0 to 300 (see fig. 1) and includes the subsonic entrance section, supersonic nozzle, and test section. The subsonic entrance section extends from stations 0 to 66 and was designed to maintain a fair wall contour between the settling chamber and the first minimum section. Since, as is customary in supersonic-nozzle design, it was assumed that the flow was uniform at the first minimum, a region of very slowly changing cross section extending from station 66 to 84 was designed to help produce the desired uniform flow. The ordinates in this section were increased by an amount intentionally insufficient to allow for full growth of the displacement thickness of the boundary layer so that choking should occur at station 84 although the geometric first minimum occurred at station 66.

The $M = 1.40$ supersonic-nozzle section was designed by the method of characteristics. In this particular application, a smoothly varying velocity distribution was assumed to exist along the center line of the nozzle from the first minimum to the beginning of the test section. The characteristic net corresponding to this velocity distribution was then established so that the wall contour required to produce uniform flow in the test section could be determined. The boundary-layer displacement thickness on the flexible wall was computed by the method given in reference 2. It was assumed that the same thickness existed on the side walls, and the combined effect of both boundary layers was then arbitrarily applied to the theoretical nozzle ordinates to satisfy the one-dimensional continuity relationship.

Test-Section Calibration

Prior to any model testing in the $M = 1.40$ nozzle, static pressures were measured along the center line of both top and bottom flexible walls, and transverse stream surveys were made at one station (see fig. 1) in the test section to determine variations of the horizontal and vertical flow angles, static pressure, and Mach number. The limits of the operating dew point required to avoid serious condensation effects were also established.

Apparatus.- Ten cruciform probes and ten pitot-static tubes similar to those shown in figure 2 and described in references 1 and 3 were used to determine flow angles and stream pressures, respectively, during the transverse survey.

Test procedure.- All test-section surveys were made for the following stagnation conditions:

Pressure, atmosphere 0.25
Dew point, °F . . . . −15 to −40
Temperature, °F 110

In an initial series of tests, the static-pressure distribution along the flexible walls was measured by means of surface orifices. The indicated Mach number distributions on the flexible walls were calculated from the ratio of the measured static pressure to the measured stagnation pressure in the settling chamber. At the completion of the wall static-pressure surveys, a transverse survey rake was installed at station 241 (fig. 1) to measure the horizontal and vertical flow angles and free-stream pressures. The survey rake was designed to support ten survey instruments, five in each of two vertical planes. Each vertical plane traversed half the tunnel width. The variation of stream angles with position and dew point was measured with ten cruciform probes installed on the survey rake. An identical series of tests was conducted with the pitot-static tubes mounted on the rake to determine free-stream pressures. This procedure was followed because it was found from previous tests (reference 1) that, although the cruciform probes indicated the correct flow angles, the indicated static pressures were too high. Data were obtained simultaneously at 2-inch transverse increments at 0, $4\frac{7}{8}$, and $9\frac{3}{4}$ inches above and below the tunnel horizontal center line.

Flow-angle variations were obtained from the cruciform-probe data by means of supersonic shock and expansion theory. The absolute angle of each probe surface in the vicinity of the orifice was measured by an optical method either prior to or after each test. These measurements were then used with the experimental angle variations to determine the absolute horizontal and vertical flow angles. The assumption made here that the probes did not deflect during the surveys is considered justified because of the small aerodynamic loads which were present and of the high rigidity of the support strut. The free-stream static pressure was obtained directly from the pitot-static-tube data and the Mach number was computed from the ratio of the total pressure behind the normal shock to the free-stream static pressure indicated by the pitot-static tubes.

Accuracy of data.- The following probable errors were estimated for the transverse survey data:

Flow-angle variation, θ_V and θ_H, degrees . . . . ±0.02
Absolute flow angle, θ_V and θ_H, degrees . . . . ±0.07
Mach number variation . . . . ±0.002
Mach number, absolute value . . . . ±0.01

Results and discussion.— Representative data presented in figure 3 show the effects of dew point on the indicated wall Mach number at several stations in the test section. In contrast to the noticeable effects of condensation which were found in the test section of the $M = 1.59$ nozzle (fig. 4, reference 1), there appears to be no measurable effect of condensation in the test section at $M = 1.40$ for the range of dew points investigated. It should be noted that these indicated Mach numbers were computed on the assumption of isentropic flow through the nozzle. Subsequent free-stream survey data indicated a nearly constant average loss of 0.2 percent of the stagnation pressure in the test section for this range of dew points. The resultant corrections would decrease the indicated wall Mach numbers by only 0.001. On the basis of these tests, the remainder of stream surveys were conducted at a dew point of -25° F.

The indicated Mach number distributions measured on the center line of the upper and lower nozzle walls at a dew point of -25° F are shown in figure 4. The theoretical Mach number distribution obtained from the two-dimensional characteristics method is also shown for comparison. The agreement is good, although the indicated Mach number in the expanding nozzle section is somewhat lower than predicted by the theory. A small asymmetry in the indicated Mach number exists between the upper and lower walls. This asymmetry is probably caused by local irregularities in the temporary mild-steel flexible walls; however, these differences are small and do not appear to affect the flow significantly. The indicated Mach numbers on the test-section walls appear in general to bracket the design Mach number of 1.40.

The results of the transverse pressure survey are presented in figures 5(a), 5(b), and 5(c), which show the variation of the horizontal flow angle, θ_H, vertical flow angle, θ_V, and Mach number, respectively, with position in the transverse plane at station 241. The ability to repeat data on two separate runs is indicated by the two sets of symbols. The tailed symbols in figure 5(a) refer to data for which the optically measured angle, a constant in this range, appears to be in error. Consequently, these data have been shifted vertically (-0.21°) to agree with the data obtained from another probe at the common point, (station 0). The variation of θ_V in figure 5(b) is large, but since the region of maximum variation is outside the normal test region for models, the aerodynamic data from model tests in this stream should not be significantly affected. Schlieren photographs of the test-section flow have been made with the schlieren system adjusted for maximum sensitivity and are shown as a composite in figure 6(b). To facilitate identification of window striae, a similar set of photographs made with the tunnel stopped are shown in figure 6(a). A comparison of the original negatives of figures 6(a) and 6(b) indicated that only one set of weak disturbances was detectable. The location of these shocks in figure 6(b) is indicated by the arrows.

The following table summarizes the flow variations in the region extending 4 inches on either side and $9\frac{3}{4}$ inches above and below the tunnel center line.

θ_H (pitch plane of model), degrees	−0.25 to 0.05
θ_V (yaw plane of model), degrees	−0.23 to 0.33
M	1.385 to 1.415

During the calibration of the $M = 1.40$ temporary nozzle, no surveys were made along the longitudinal center line. The Mach number and flow-angle variations in the region of the model installation (stations 235 to 265) were, therefore, computed from the transverse survey data and are shown in figure 7. The validity of these computations is discussed in reference 1 where the agreement between the computed and measured axial variations is good. The variation of flow angle in the vicinity of the fuselage is in general good except near the rear of the body. The maximum variation of θ_H from stations 235 to 265 is -0.24° to 0.19° and of θ_V from stations 231.4 to 250.6 is 0.27° to -0.11°. The Mach number variation is 1.395 to 1.407. On the basis of these calculations and the transverse survey data, the test Mach number is considered to be 1.40. The flow in the test section is not so uniform as would be ultimately desired. It is believed, however, that the variations present in the vicinity of the model will not unduly affect the proposed tests and that the flow is suitable for aerodynamic testing. The temporary nature of this nozzle did not warrant any extensive attempts to improve the flow characteristics in the test section.

MODEL AND INSTALLATION

The test model was constructed from steel to coordinates presented in table I and is shown in figure 8. This is the same model used for the tests reported in reference 1. The basic model (without canopies) is a body of revolution having an over-all length of 30.267 inches and a fineness ratio of 9.4. The top and bottom canopies are removable so that the fuselage can be tested as a body of revolution. The rear part of the fuselage is integral with the supporting sting which had a 3° cone angle beginning at the rear of the model. The pressure orifices were located at various radial positions at nine basic stations of the model as shown in figure 8. In addition, one comprehensive longitudinal row of orifices was located along the upper surface ($\phi = 180^{\circ}$) of the basic body (no canopies). For the fuselage with canopies installed, the orifices located at approximately 150° were relocated at the canopy juncture. The pressures were photographically recorded from multiple-tube manometers filled with Alkazene 42 (x-dibromoethylbenzene). This manometer fluid, having a specific gravity of approximately 1.75, was found particularly suited for these tests because of its extremely low vapor pressure and low viscosity.

The installation of the body of revolution in the tunnel is shown in figure 9. A scale drawing of the installation showing principal dimensions is presented in figure 10. The angle of attack was varied in a horizontal plane through fixed increments by rotating the model about the 59-percent position of the fuselage.

TESTS, CORRECTIONS, AND ACCURACY

Tests

The basic pressure data were obtained for the fuselage as a body of revolution and with canopies for an angle-of-attack range from -5° to 10° at a Mach number of 1.40 and a Reynolds number of 2.7×10^6 based on the fuselage length. This Reynolds number and Mach number condition corresponds to full-scale similarity at an altitude of approximately 110,000 feet. The aerodynamic data were obtained at tunnel stagnation conditions of: pressure, 0.25 atmosphere; temperature, 110° F; and dew point, -25° F.

Corrections and Accuracy

Since the magnitude of the flow angle, Mach number, and pressure-coefficient gradients are in general small in the vicinity of the model, no corrections have been applied to the data. The variation of the test conditions and accuracy of the data are estimated to be as follows:

Mach number	±0.01
Angle of attack, degrees:	
Geometric measurement (probable error)	±0.02
Flow irregularity (θ_H)	$\begin{cases} 0.24 \\ -0.19 \end{cases}$
Angle of yaw, degrees:	
Flow irregularity (θ_V)	$\begin{cases} 0.27 \\ -0.11 \end{cases}$
Absolute pressure coefficient	±0.012
Variation of radial pressure coefficient	±0.005

PRESENTATION OF RESULTS

The basic data obtained from the tests of the body of revolution and complete fuselage are presented in figures 11 and 12, respectively. The pressure coefficient, P, is plotted against the radial angle, ϕ, for nine stations along the body. The fact that the radial data at some of the stations are incomplete is due to plugged orifices and tubes. Two sets of data were recorded consecutively for each model position. However, in general, only one set has been plotted. The plotted data are tabulated in tables II and IV and the supplementary data including data for other angles of attack are tabulated in tables III and V. Figure 11 also includes representative theoretical curves for six axial stations and for angles of attack of -5°, 0°, and 10°. The theoretical results have been omitted at stations 46.2 and 73.1 because the orifices at these stations were located in a region where the change in body slope is discontinuous and the exact slope is not known. The theoretical results have been omitted at station 93.5 because of sting interference effects on the experimental results. In calculating the theoretical curves, the linearized theory has been used in rigorous form (see section entitled "Discussion").

The same basic data for the body of revolution are replotted in figure 13 as a function of $\alpha \cos \phi$, a parameter which as been commonly used in both linear and nonlinear theoretical methods. In this figure results for both the rigorous and incomplete linear theory are also presented in order to establish the exact magnitudes of the discrepancies between both theoretical results. In addition, in figure 13, the nonlinear theoretical results are presented for station 5.6, which is on the conical nose section of the body, for 0° angle of attack as obtained from reference 4 and for angles of attack as obtained from reference 5.

The axial pressure distribution along the body for $\phi = 180^{\circ}$ and 0° angle of attack is presented in figure 14 for comparison with the results of both the rigorous and incomplete linear solutions. In addition, the nonlinear theoretical solution obtained by the method of characteristics (see, for example, reference 6) is also presented in figure 14. In this application of the method of characteristics the effects of shock curvature have been neglected since, as pointed out in reference 1, it is estimated that these effects are small. Figure 15 presents a comparison of the axial pressure distribution at $\phi = 180^{\circ}$ with the rigorous linear theory for several angles of attack.

In figure 16, the pressures measured over the top canopy ($\phi = 180^{\circ}$) for 0° angle of attack are compared with the results of two approximations (discussed in reference 1) for estimating the pressures. The pressure distribution over the canopy at several angles of attack is plotted in figure 17. The data presented in figures 14 and 15, 16 and 17 are tabulated in tables VI and VIII, respectively. Similar supplementary data, together with data for other angles of attack, are given in tables VII and IX.

DISCUSSION

Considerable effort has been directed towards unifying the results of the linear theory as applied to bodies of revolution and towards establishing these results rigorously consistent with the assumptions of the linearization. Lighthill, in reference 7, presents the linearized form of the pressure coefficient as:

$$P = -\frac{2u}{V} - \left(\frac{v}{V}\right)^2 \tag{1}$$

In investigating the flow about inclined bodies of revolution, H. J. Allen of the Ames Aeronautical Laboratory has recently applied equation (1) to obtain a solution of the form:

$$P_\alpha = P'_{\alpha=0} + \Delta P' \alpha \cos \phi + (1 - 4 \sin^2\phi)\alpha^2 \tag{2}$$

where $P'_{\alpha=0}$ is the zero-angle-of-attack solution. Hence, in order to compare the experimental results of the present investigation with theory, the linearized pressure coefficient was obtained from equation (2) with the term $P'_{\alpha=0}$ evaluated consistent with equation (1). In determining $P'_{\alpha=0}$ and $\Delta P'$, the step process of Von Kármán and Moore (reference 8) was used for 0° angle of attack, and of Tsien (reference 9) for angle of attack. Since in the past the pressure coefficient has been commonly determined with the omission of the term $(v/V)^2$ in equation (1) and consequently with the omission of $(1 - 4 \sin^2\phi)\alpha^2$ in equation (2), the magnitude and influence of these two terms will be considered in the results presented in figures 13 and 14. In figure 13, the pressure data have been plotted against the parameter $\alpha \cos \phi$ which has been significant in both the incomplete linear solution and the nonlinear solution for small angles of attack (reference 6). The large discrepancies between the rigorous linear theory and the incomplete linear theory (a single curve applying for all angles of attack) shown in figure 13 clearly indicate the importance of the omitted terms.

In considering the general nonlinear theoretical solution for bodies of revolution at small yaw, the pressure coefficient has the form:

$$P = P_{\alpha=0} + \Delta P \alpha \cos \phi \tag{3}$$

where $P_{\alpha=0}$ is the theoretical nonlinear pressure coefficient at 0° angle of attack and ΔP depends upon the body geometry, free-stream Mach number, and shock curvature. If the effects of shock curvature are negligible, then ΔP is independent of the angle of attack and the nonlinear solution, equation (3), has the identical form as the incomplete linear solution. If shock curvature effects are not negligible, then the form remains the same with, however, ΔP becoming a function of the angle of attack. Hence, if equation (3) were applied to the cylindrical portion of a body of revolution at large distances from the nose, then ΔP would tend to vanish and the pressure would be a constant independent of the radial position. However, from a physical consideration, the incompressible distribution about a circular cylinder would be expected for small angles of attack if the rotation in the flow is vanishingly small. Such a result is given by the rigorous linear theory (equation (2)). It, therefore, appears that an angle-of-attack term of the order of α^2, which is of the same order as the term $\Delta P\alpha$, has been omitted from the general nonlinear solution presented by equation (3). The importance of this term in affecting the pressure-distribution prediction can be seen from the curved nature of the experimental data when plotted against $\alpha \cos \phi$ (fig. 13).

A general comparison of the experimental and rigorous linear theoretical results (fig. 11) indicates, with the possible exception of the first station, very good agreement for all angles of attack as far back as station 84.3 (last station available for comparison). At the first station, 5.6, the primary discrepancy occurs in predicting the zero-angle-of-attack value since the theoretical variations accurately agree with the experimental radial variations. This discrepancy for the cone value is somewhat more evident from the zero-angle-of-attack data of figure 13. By coincidence, the incomplete solution agrees much more closely with the characteristic solution than the rigorous linear solution.

The importance of using the rigorous solution becomes readily apparent from an examination of figure 13. In this comparison, as previously pointed out, the incomplete linear solution is represented by a single curve. It becomes immediately apparent that a straight line will not predict the general nature of the experimental curves and that the rigorous linear theory in general excellently predicts both the magnitude and shape of the experimental curves as far back as the limit of comparison of the present tests. In comparing the nonlinear solution for the yawed cone (references 4 and 5) at station 5.6, it can be seen that the theory gives a very good prediction for small angles of attack but becomes progressively worse as the angle increases. It appears, then, that the cone solution is restricted to angles of yaw which are small compared to the cone angle.

The axial pressure distributions at $\phi = 180^\circ$ presented in figures 14 and 15 are typical of the agreement between the experimental and rigorous-linear-theory results at any radial station (see fig. 11). Figure 14 shows the relative importance of the $(v/V)^2$ term in determining the pressure distribution at 0° angle of attack. Since over most of the body the magnitude of this term is small, both the rigorous and incomplete solutions are essentially the same over more than half the body. The maximum discrepancy occurs in the vicinity of the nose, as previously noted, where the perturbations are large. Over the rear 10 percent of the body, the effects of boundary-layer separation caused or aided by sting interference prevent the rapid expansion predicted by theory. As can be seen from figure 15, the agreement between the theory and experimental results is good even at high angles of attack.

It should be pointed out that the use of the rigorous linear theory in predicting the lift or moment characteristics of bodies of revolution will give the same results as the use of the incomplete theory since the integrated effects of the α^2 term are exactly zero.

The effects of the canopies on the fuselage pressure distribution can be seen by comparing figures 11 and 12. It appears that the shock from the top canopy crosses station 10.9 in the region of $\phi = 90^\circ$ since the pressures at $\phi = 60^\circ$ at this station are the same for the fuselage with and without canopies. (The differences in the distributions at station 5.6 for the two configurations is considered to be an experimental error of an undetermined origin.) At station 22.0 and farther rearward, the canopy effects are noticeable over the entire body. The pressure distributions on the top canopy at $\phi = 180^\circ$ are shown in figures 16 and 17, and indicate the expected trends. After the initial compression and expansion on the front of the canopy, the pressures approach zero. The results of the approximations (fig. 16) were obtained by methods described in reference 1 and are reviewed briefly here. The first method makes the assumption that the canopy extends completely around the body of revolution and computes the resultant pressure distribution by means of the rigorous linear theory. Similarly, the second method assumes that the canopy windshield is a cone whose axis is an element of the conical nose section of the fuselage and that the Mach number ahead of the cone is the same as that on the surface of the fuselage nose section. It is realized that these assumptions are crude. However, a combination of the two methods does give a reasonable estimate of the pressures to be expected on the canopy.

CONCLUSIONS

Pressure-distribution tests of a supersonic-aircraft fuselage with and without canopies have been conducted in the Langley 4- by 4-foot supersonic tunnel at a Mach number of 1.40 and a Reynolds number of 2.7×10^6. These data, which were obtained upon completion of a series of calibration tests of the $M = 1.40$ nozzle, are compared with linear and nonlinear theoretical results. The following conclusions are indicated from the calibration and pressure-distribution tests:

1. The test-section flow in the vicinity of the model is considered sufficiently uniform to be suitable for aerodynamic testing.

2. A general comparison of the experimental pressure distributions with rigorous linear theory indicates, with the possible exception of the nose cone, very good agreement between the experimental and theoretical pressures for the test angle-of-attack range (-5° to 10°) up to the last station (84.3 percent of fuselage length) at which complete experimental data were available. The discrepancy at the nose is limited to the prediction of the pressure coefficient at zero angle of attack.

3. A comparison of the rigorous and the incomplete linear theory with experimental data clearly indicates the importance of the radial perturbation velocity which is neglected in the incomplete theory.

4. Nonlinear solutions for the pressures about arbitrary bodies of revolution which have the same form of solution as the incomplete linear theory appear to be inadequate in the same respects as the incomplete linear solutions.

Langley Aeronautical Laboratory
National Advisory Committee for Aeronautics
Langley Air Force Base, Va.

REFERENCES

1. Cooper, Morton, Smith, Norman F., and Kainer, Julian H.: A Pressure-Distribution Investigation of a Supersonic Aircraft Fuselage and Calibration of the Mach Number 1.59 Nozzle of the Langley 4- by 4-Foot Supersonic Tunnel. NACA RM L9E27a, 1949.

2. Tetervin, Neal: Approximate Formulas for the Computation of Turbulent Boundary-Layer Momentum Thicknesses in Compressible Flows. NACA ACR L6A22, 1946.

3. Hasel, Lowell E., and Coletti, Donald E.: Investigation of Two Pitot-Static Tubes at Supersonic Speeds. NACA RM L8I02, 1948.

4. Staff of the Computing Section, Center of Analysis (Under Direction of Zdeněk Kopal): Tables of Supersonic Flow around Cones. Tech. Rep. No. 1, M.I.T., 1947.

5. Staff of the Computing Section, Center of Analysis (Under Direction of Zdeněk Kopal): Tables of Supersonic Flow around Yawing Cones. Tech. Rep. No. 3, M.I.T., 1947

6. Ferri, Antonio: Application of the Method of Characteristics to Supersonic Rotational Flow. NACA Rep. 841, 1946.

7. Lighthill, M. J.: Methods for Predicting Phenomena in the High-Speed Flow of Gases. Jour. Aero. Sci., vol. 16, no. 2, Feb. 1949, pp. 69-83.

8. Von Kármán, Theodor, and Moore, Norton B.: Resistance of Slender Bodies Moving with Supersonic Velocities, with Special Reference to Projectiles. Trans. A.S.M.E., vol. 54, no. 23, Dec. 15, 1932, pp. 303-310.

9. Tsien, Hsue-Shen: Supersonic Flow over an Inclined Body of Revolution. Jour. Aero. Sci., vol. 5, no. 12, Oct. 1938, pp. 480-483.

TABLE I.- FUSELAGE AND CANOPY MODEL COORDINATES

(See fig. 8)

Streamline body (in.)

Station	Radius
0	0
2.480	.638
3.396	.852
4.262	1.030
5.134	1.174
5.778	1.252
6.328	1.290
11.800	1.517
12.172	1.532
13.952	1.606
22.020	1.606
23.374	1.549
23.644	1.538
24.310	1.510
24.976	1.482
25.308	1.468
25.782	1.448
26.308	1.426
27.025	1.385
27.640	1.350
28.972	1.186
30.267	.900

Top canopy (in.)

Station 2.964		Station 4.262		Station 5.128		Station 6.560		Stations 13.952 to 22.020	
x	y	x	y	x	y	x	y	x	y
0	0.872	0	1.432	0	1.814	0	2.030	0	2.032
.126	.800	.132	1.408	.132	1.794	.132	2.016	.266	1.964
.214	.722	.266	1.320	.266	1.736	.266	1.968	.392	1.864
		.400	1.180	.400	1.626	.400	1.882	.532	1.664
		.574	.856	.532	1.424	.532	1.722	.612	1.482
				.684	.956	.598	1.596		
						.666	1.376		
						.720	1.066		

Station 23.374		Station 23.644		Station 24.310		Station 24.976		Station 25.308		Station 25.782	
x	y	x	y	x	y	x	y	x	y	x	y
0	2.032	0	2.027	0	2.010	0	2.002	0	1.977	0	1.920
.256	1.964	.246	1.964	.352	1.864	.322	1.864	.304	1.856	.188	1.864
.378	1.864	.370	1.864	.460	1.664	.416	1.664	.388	1.664	.320	1.664
.503	1.664	.491	1.664	.500	1.482	.444	1.482	.404	1.482	.344	1.482
.570	1.440	.556	1.436	.505	1.424	.447	1.414	.405	1.411	.354	1.404

Bottom canopy (in.)

Station 5.994		Station 8.892		Stations 12.172 to 22.152		Station 24.310		Station 26.640	
x	y	x	y	x	y	x	y	x	y
0	1.398	0	1.788	0	2.080	0	1.878	0	1.510
.066	1.392	.066	1.784	.066	2.080	.132	1.854	.132	1.494
.132	1.372	.132	1.768	.132	2.076	.266	1.776	.266	1.416
.198	1.338	.198	1.736	.198	2.068	.400	1.584	.308	1.372
.266	1.282	.266	1.688	.266	2.028	.490	1.428		
.306	1.232	.334	1.614	.334	1.954				
		.400	1.472	.400	1.824				
		.462	1.316	.466	1.684				
				.550	1.508				

NACA

TABLE II.– PRESSURE-COEFFICIENT DATA PRESENTED IN FIGURE 11 FOR

THE FUSELAGE AS A BODY OF REVOLUTION

Station (percent)	Radial angle, ϕ	Angle of attack (deg)						
		-5	0	2	4	6	8	10
5.6	0	0.170	0.236	0.272	0.305	0.345	0.386	0.431
	60	.204	.244	.256	.259	.265	.268	.267
	90	.248	.250	.244	.227	.215	.196	.175
	120	.286	.242	.220	.194	.174	.148	.119
	180	.330	.242	.208	.180	.158	.136	.119
10.9	0	.103	.166	.196	.227	.265	.306	.346
	60	.119	.164	.181	.188	.200	.204	.206
	90	.151	.164	.165	.156	.146	.128	.106
	120	.194	.162	.149	.128	.108	.080	.050
	180	.230	.152	.125	.104	.084	.064	.042
22.0	0	-.110	-.081	-.062	-.044	-.019	.004	.031
	60	-.114	-.077	-.069	-.068	-.063	-.065	-.073
	120	-.065	-.077	-.085	-.094	-.117	-.137	-.165
	147	-.045	-.077	-.091	-.108	-.117	-.127	-.145
	180	-.031	-.079	-.093	-.106	-.113	-.119	-.125
34.6	0	-.029	-.026	-.018	-.013	.004	.024	.043
	60	-.045	-.024	-.022	-.028	-.033	-.044	-.059
	90	-.045	-.024	-.026	-.036	-.049	-.071	-.107
	120	-.033	-.026	-.026	-.036	-.047	-.069	-.103
	153	-.011	-.028	-.030	-.034	-.039	-.040	-.035
	180	-.001	-.022	-.028	-.030	-.027	-.020	-.017
46.2	0	-.061	-.056	-.050	-.044	-.031	-.018	-.007
	90	-.082	-.058	-.062	-.076	-.093	-.119	-.151
	120	-.067	-.050	-.060	-.070	-.075	-.095	-.123
	180	-.027	-.046	-.046	-.050	-.051	-.054	-.047
59.7	0	-.021	-.028	-.026	-.028	-.019	-.012	-.005
	90	-.041	-.020	-.022	-.032	-.049	-.075	-.099
	120	-.035	-.018	-.020	-.032	-.049	-.054	-.075
	158	-.019	-.022	-.020	-.022	-.017	-.018	-.035
	180	-.011	-.022	-.022	-.018	-.011	-.004	-.003
73.1	0	-.059	-.050	-.063	-.066	-.059	-.054	-.047
	60	-.061	-.058	-.058	-.068	-.075	-.087	-.109
	90	-.081	-.058	-.062	-.076	-.085	-.105	-.133
	120	-.077	-.058	-.058	-.070	-.069	-.081	-.105
	158							
	180	-.049	-.058	-.054	-.058	-.047	-.046	-.049
84.3	0	-.021	-.048	-.048	-.054	-.053	-.050	-.045
	60	-.045	-.046	-.046	-.058	-.069	-.085	-.105
	90	-.069	-.046	-.048	-.060	-.071	-.089	-.105
	120	-.065	-.046	-.046	-.046	-.045	-.063	-.089
93.5	120	-.156	-.061	-.077	-.131	-.127	-.147	-.165

NACA

TABLE III.– SUPPLEMENTARY PRESSURE-COEFFICIENT DATA FOR

THE FUSELAGE AS A BODY OF REVOLUTION

Station (percent)	Radial angle, ϕ	Angle of attack (deg)										
		–5	–3	–3	–2	–2	0	2	4	6	8	10
5.6	0	0.170	0.195	0.191	0.208	0.210	0.238	0.272	0.305	0.346	0.386	0.430
	60	.204	.219	.219	.228	.230	.244	.256	.262	.266	.268	.268
	90	.247	.250	.249	.254	.256	.250	.244	.230	.217	.196	.176
	120	.285	.266	.267	.260	.262	.242	.224	.194	.175	.148	.120
	180	.331	.292	.290	.278	.277	.242	.208	.182	.159	.138	.116
10.9	0	.104	.123	.124	.139	.140	.166	.198	.230	.266	.306	.347
	60	.120	.139	.140	.149	.150	.164	.181	.190	.199	.204	.207
	90	.152	.159	.159	.162	.166	.164	.167	.155	.147	.128	.107
	120	.192	.181	.179	.178	.178	.162	.149	.127	.109	.080	.051
	180	.231	.197	.195	.186	.182	.150	.125	.103	.085	.066	.047
22.0	0	–.111	–.103	–.102	–.093	–.092	–.081	–.062	–.044	–.018	.006	.032
	60	–.107	–.097	–.094	–.089	–.086	–.077	–.069	–.067	–.064	–.063	–.070
	120	–.065	–.071	–.070	–.073	–.070	–.077	–.085	–.101	–.118	–.137	–.162
	147	–.043	–.061	–.062	–.069	–.064	–.079	–.091	–.107	–.118	–.127	–.142
	180	–.029	–.053	–.052	–.061	–.060	–.077	–.093	–.103	–.112	–.117	–.130
34.6	0	–.029	–.030	–.031	–.029	–.025	–.024	–.018	–.012	.004	.024	.044
	60	–.041	–.034	–.035	–.029	–.027	–.024	–.022	–.028	–.034	–.044	–.056
	90	–.043	–.032	–.033	–.027	–.025	–.024	–.026	–.036	–.050	–.071	–.106
	120	–.031	–.028	–.027	–.025	–.021	–.026	–.028	–.036	–.048	–.069	–.100
	153	–.009	–.020	–.019	–.021	–.021	–.028	–.030	–.034	–.040	–.040	–.030
	180	.001	–.012	–.011	–.017	–.015	–.022	–.028	–.030	–.028	–.018	–.022
46.2	0	–.061	–.060	–.059	–.059	–.056	–.056	–.050	–.044	–.032	–.018	–.006
	90	–.081	–.070	–.071	–.065	–.062	–.058	–.062	–.075	–.094	–.119	–.148
	120	–.065	–.062	–.063	–.059	–.056	–.050	–.062	–.069	–.076	–.095	–.118
	180	–.025	–.036	–.037	–.037	–.035	–.046	–.046	–.048	–.052	–.054	–.052
59.7	0	–.019	–.026	–.027	–.025	–.023	–.028	–.026	–.026	–.020	–.012	–.002
	90	–.043	–.030	–.029	–.025	–.021	–.020	–.026	–.032	–.050	–.075	–.094
	120	–.033	–.026	–.027	–.021	–.021	–.020	–.020	–.032	–.048	–.052	–.072
	158	–.017	–.022	–.023	–.021	–.017	–.022	–.020	–.022	–.018	–.018	–.030
	180	–.011	–.018	–.019	–.021	–.017	–.022	–.022	–.016	–.010	–.002	–.006
73.1	0	–.057	.066	–.067	–.061	–.058	–.050	–.063	–.063	–.058	–.054	–.044
	60	–.061	.062	–.063	–.061	–.056	–.058	–.058	–.067	–.076	–.087	–.106
	90	–.079	.070	–.071	–.063	–.062	–.058	–.062	–.075	–.086	–.105	–.130
	120	–.075	.066	–.067	–.061	–.060	–.058	–.058	–.069	–.068	–.081	–.102
	180	–.047	.054	–.055	–.055	–.052	–.058	–.054	–.056	–.048	–.046	–.048
84.3	0	–.019	–.036	–.035	–.041	–.037	–.046	–.046	–.054	–.054	–.050	–.044
	60	–.043	–.054	–.055	–.045	–.044	–.046	–.046	–.056	–.070	–.085	–.106
	90	–.067	–.058	–.057	–.049	–.046	–.046	–.046	–.060	–.072	–.085	–.106
	120	–.065	–.054	–.055	–.049	–.046	–.044	–.046	–.046	–.044	–.063	–.090
93.5	120	–.159	–.143	–.146	–.093	–.088	–.061	–.075	–.131	–.127	–.147	–.164

NACA

TABLE IV.– PRESSURE-COEFFICIENT DATA PRESENTED IN FIGURE 12

FOR THE COMPLETE FUSELAGE

Station (percent)	Radial angle, ϕ	Angle of attack (deg)						
		–5	0	2	4	6	8	10
5.6	0	0.169	0.244	0.276	0.311	0.352	0.395	0.437
	60	.201	.252	.260	.274	.286	.295	.304
	90	.241	.256	.248	.240	.231	.217	.196
	120	.278	.246	.222	.202	.181	.158	.128
	180	.332	.244	.206	.179	.157	.138	.118
10.9	0	.101	.166	.192	.226	.264	.305	.345
	60	.123	.166	.176	.188	.199	.206	.206
	90	.171	.180	.172	.163	.149	.132	.106
	120	.248	.220	.200	.181	.163	.136	.108
	180	.461	.363	.328	.298	.270	.243	.214
22.0	0	–.102	–.064	–.047	–.026	0	.024	.054
	60	–.078	–.032	–.025	–.020	–.016	–.013	–.028
	120	–.106	–.092	–.087	–.087	–.090	–.097	–.106
	147	–.139	–.152	–.156	–.161	–.161	–.159	–.162
	180	–.143	–.184	–.190	–.202	–.219	–.226	–.238
34.6	0	–.046	–.020	–.007	.010	.030	.052	.076
	60	–.042	–.032	–.035	–.034	–.036	–.039	–.044
	90	–.046	–.034	–.045	–.062	–.082	–.107	–.132
	120	–.034	–.026	–.037	–.058	–.074	–.097	–.126
	153	–.018	–.040	–.035	–.048	–.054	–.063	–.068
	180	–.030	–.040	–.039	–.038	–.034	–.023	–.014
46.2	0	–.052	–.044	–.039	–.032	–.020	–.007	.012
	90	–.086	–.068	–.073	–.093	–.112	–.141	–.174
	120	–.066	–.060	–.067	–.079	–.094	–.117	–.132
	158	0	–.016	–.025	–.034	–.036	–.033	–.034
	180	.014	.020	.001	0	–.002	–.001	–.006
59.7	0	–.030	–.032	–.033	–.034	–.028	–.019	–.012
	90	–.038	–.006	–.009	–.020	–.034	–.057	–.084
	120	–.036	–.008	–.009	–.016	–.022	–.031	–.040
	158	–.018	–.020	–.019	–.020	–.016	–.015	–.016
	180	–.010	–.020	–.027	–.020	–.016	–.013	–.012
73.1	0	–.052	–.046	–.043	–.042	–.036	–.027	–.020
	60	–.068	–.050	–.051	–.058	–.066	–.079	–.096
	90	–.082	–.058	–.059	–.069	–.084	–.101	–.126
	120	–.068	–.056	–.057	–.065	–.062	–.079	–.084
	158	–.014	–.014	–.019	–.026	–.018	–.031	–.040
	180	–.002	–.006	–.013	–.012	–.008	–.001	–.004
84.3	0	–.036	–.046	–.051	–.058	–.056	–.065	–.064
	60	–.066	–.050	–.053	–.062	–.070	–.083	–.102
	90	–.082	–.056	–.055	–.063	–.074	–.083	–.106
	120	–.082	–.058	–.063	–.067	–.074	–.079	–.086
93.5	0	–.145	–.120	–.116	–.119	–.114	–.111	–.122

TABLE V.– SUPPLEMENTARY PRESSURE–COEFFICIENT DATA FOR

THE COMPLETE FUSELAGE

Station (percent)	Radial angle, ø	Angle of attack (deg)										
		–5	–3	–3	–2	–2	0	2	4	6	8	10
5.6	0	0.171	0.196	0.195	0.213	0.211	0.245	0.275	0.311	0.349	0.397	0.439
	60	.202	.223	.223	.233	.233	.249	.263	.273	.283	.297	.304
	90	.242	.249	.251	.253	.253	.257	.249	.240	.228	.217	.198
	120	.280	.267	.265	.261	.261	.247	.223	.202	.178	.158	.128
	180	.331	.293	.293	.277	.277	.243	.208	.178	.154	.138	.120
10.9	0	.101	.124	.125	.137	.137	.165	.194	.228	.262	.307	.347
	60	.125	.144	.141	.153	.153	.167	.178	.188	.196	.206	.206
	90	.173	.178	.177	.181	.179	.181	.174	.162	.146	.132	.106
	120	.248	.239	.239	.235	.235	.221	.202	.180	.160	.138	.110
	180	.462	.423	.421	.405	.403	.365	.329	.297	.268	.243	.214
22.0	0	–.101	–.089	–.090	–.081	–.080	–.065	–.045	–.027	–.001	.024	.056
	60	–.077	–.055	–.056	–.047	–.048	–.035	–.023	–.021	–.017	–.015	–.026
	120	–.105	–.099	–.100	–.095	–.096	–.091	–.087	–.088	–.092	–.097	–.106
	147	–.137	–.147	–.146	–.149	–.148	–.153	–.155	–.162	–.162	–.159	–.164
	180	–.143	–.163	–.162	–.169	–.168	–.183	–.187	–.203	–.221	–.226	–.236
34.6	0	–.046	–.037	–.038	–.031	–.032	–.021	–.005	.009	.029	.052	.078
	60	–.040	–.037	–.040	–.035	–.034	–.033	–.033	–.035	–.037	–.039	–.044
	90	–.046	–.035	–.034	–.031	–.028	–.035	–.043	–.062	–.084	–.105	–.130
	120	–.032	–.031	–.032	–.023	–.024	–.027	–.037	–.058	–.076	–.095	–.124
	153	–.016	–.031	–.034	–.037	–.036	–.039	–.033	–.046	–.054	–.063	–.066
	180	–.030	–.035	–.038	–.037	–.038	–.041	–.037	–.039	–.035	–.023	–.012
46.2	0	–.050	–.047	–.050	–.047	–.048	–.043	–.037	–.033	–.023	–.007	.014
	90	–.083	–.075	–.076	–.071	–.070	–.067	–.071	–.094	.114	–.141	–.174
	120	–.063	–.059	–.060	–.059	–.058	–.059	–.065	–.080	–.094	–.117	–.130
	158	.002	–.003	–.004	–.007	–.006	–.019	–.023	–.035	–.039	–.033	–.034
	180	.016	.006	.006	.013	.014	.019	.002	–.001	–.005	–.001	–.004
59.7	0	–.030	–.031	–.032	–.033	–.034	–.033	–.031	–.035	–.029	–.019	–.010
	90	–.036	–.031	–.018	–.011	–.012	–.007	–.007	–.021	–.037	–.055	–.084
	120	–.034	–.015	–.020	–.015	–.016	–.011	–.007	–.017	–.025	–.031	–.040
	158	–.018	–.019	–.022	–.019	–.020	–.019	–.017	–.019	–.019	–.015	–.016
	180	–.010	–.015	–.018	–.019	–.018	–.021	–.025	–.021	–.019	–.011	–.010
73.1	0	–.050	–.051	–.050	–.049	–.048	–.047	–.041	–.040	–.037	–.027	–.018
	60	–.065	–.059	–.058	–.055	–.054	–.051	–.049	–.058	–.066	–.079	–.094
	90	–.077	–.067	–.066	–.063	–.062	–.059	–.057	–.070	–.084	–.101	–.124
	120	–.065	–.059	–.062	–.059	–.058	–.055	–.057	–.066	–.070	–.077	–.084
	158	–.016	–.017	–.018	–.015	–.018	–.017	–.017	–.027	–.027	–.031	–.040
	180	0	–.003	–.006	–.007	–.008	–.007	–.011	–.019	–.011	–.001	–.004
84.3	0	–.034	–.039	–.040	–.041	–.040	–.047	–.049	–.058	–.050	–.063	–.064
	60	–.063	–.059	–.058	–.053	–.056	–.051	–.051	–.062	–.062	–.083	–.102
	90	–.077	–.063	–.066	–.059	–.060	–.057	–.053	–.064	–.066	–.087	–.106
	120	–.079	–.069	–.070	–.063	–.064	–.059	–.061	–.068	–.066	–.079	–.084
93.5	0	–.145	–.133	–.134	–.127	–.128	–.121	–.115	–.120	–.108	–.115	–.120

TABLE VI.– PRESSURE-COEFFICIENT DATA PRESENTED IN FIGURES 14 AND 15 AT POSITION $\phi = 180^{\circ}$ ON THE BODY OF REVOLUTION

Station (percent)	Angle of attack (deg)				
	–5	0	2	6	10
1.7	0.338	0.250	0.218	0.164	0.123
5.6	.330	.242	.208	.158	.119
8.5	.314	.224	.194	.142	.107
11.0	.230	.152	.125	.084	.047
15.4	.155	.086	.061	.020	–.015
16.8	.093	.030	.006	–.029	–.059
19.9	–.005	–.060	–.073	–.101	–.111
22.0	–.031	–.079	–.093	–.113	–.125
24.4	–.021	–.065	–.075	–.089	–.099
27.3	–.013	–.046	–.054	–.065	–.065
34.7	–.001	–.022	–.028	–.027	–.017
38.7	.011	–.006	–.012	–.011	–.005
44.8	–.001	–.026	–.034	–.033	–.029
46.3	–.027	–.046	–.046	–.051	–.047
47.5	–.045	–.058	–.060	–.065	–.065
52.5	–.037	–.048	–.044	–.037	–.021
59.7	–.011	–.022	–.022	–.011	–.003
65.0	.003	–.010	–.008	.002	.005
71.5	–.005	–.022	–.018	–.003	–.003
73.2	–.049	–.058	–.054	–.047	–.049
74.5	–.065	–.065	–.058	–.059	–.067
79.0	–.049	–.050	–.036	–.029	–.039
84.1	–.047	–.042	–.032	–.015	–.031
86.0	–.041	–.038	–.028	–.005	–.019
90.0	–.085	–.069	–.063	–.049	–.059
93.5	–.156	–.065	–.089	–.123	–.155
96.0	–.122	–.060	–.073	–.131	–.171

TABLE VII.- SUPPLEMENTARY PRESSURE-COEFFICIENT DATA AT POSITION

$\phi = 180^{\circ}$ ON THE BODY OF REVOLUTION

Station (percent)	Angle of attack (deg)												
	−5	−3	−3	−2	−2	0	2	4	4	6	8	8	10
1.7	0.339	0.300	0.300	0.294	0.287	0.250	0.218	0.188	0.190	0.165	0.140	0.140	0.120
5.6	.331	.292	.290	.278	.277	.242	.208	.180	.182	.159	.136	.138	.116
8.5	.315	.274	.275	.266	.264	.226	.194	.168	.167	.143	.124	.124	.102
11.0	.231	.197	.195	.186	.182	.150	.125	.104	.103	.085	.064	.066	.042
15.4	.156	.123	.124	.123	.118	.086	.061	.039	.040	.022	.008	.002	−.018
16.8	.094	.065	.064	.053	.055	.030	.006	−.014	−.012	−.030	−.044	−.044	−.064
19.9	−.003	−.028	−.029	−.037	−.033	−.060	−.073	−.090	−.087	−.102	−.107	−.109	−.118
22.0	−.029	−.052	−.053	−.061	−.060	−.077	−.093	−.106	−.103	−.112	−.119	−.117	−.130
24.4	−.023	−.042	−.043	−.051	−.048	−.065	−.075	−.084	−.083	−.090	−.095	−.095	−.102
27.3	−.011	−.030	−.029	−.033	−.033	−.046	−.054	−.060	−.060	−.064	−.067	−.067	−.068
34.7	.001	−.012	−.011	−.017	−.015	−.022	−.028	−.030	−.030	−.028	−.020	−.018	−.022
38.7	.012	0	.001	−.005	−.001	−.006	−.012	−.014	−.014	−.010	−.008	−.008	−.010
44.8	.001	−.012	−.013	−.017	−.017	−.026	−.034	−.036	−.036	−.034	−.034	−.032	−.032
46.3	−.025	−.036	−.037	−.037	−.035	−.046	−.046	−.050	−.048	−.052	−.054	−.054	−.052
47.5	−.043	−.054	−.055	−.057	−.054	−.058	−.060	−.062	−.060	−.066	−.067	−.067	−.068
52.5	−.035	−.042	−.043	−.043	−.040	−.048	−.044	−.042	−.040	−.038	−.032	−.032	−.026
59.7	−.011	−.018	−.019	−.021	−.017	−.022	−.022	−.018	−.016	−.010	−.004	−.002	−.006
65.0	.002	−.004	−.005	−.005	−.001	−.010	−.004	−.007	−.006	.002	.010	.010	.006
71.5	−.005	−.012	−.013	−.009	−.009	−.022	−.018	−.014	−.016	−.004	0	0	−.004
73.2	−.047	−.054	−.055	−.055	−.052	−.058	−.054	−.058	−.056	−.048	−.046	−.046	−.048
74.5	−.063	−.066	−.067	−.065	−.062	−.065	−.058	−.062	−.062	−.060	−.063	−.061	−.068
79.0	−.047	−.050	−.051	−.049	−.046	−.048	−.040	−.036	−.036	−.030	−.030	−.030	−.038
84.1	−.045	−.044	−.047	−.041	−.040	−.042	−.034	−.028	−.028	−.016	−.022	−.022	−.030
86.0	−.039	−.038	−.039	−.035	−.033	−.036	−.028	−.018	−.016	−.004	−.008	−.008	−.018
90.0	−.079	−.078	−.079	−.073	−.072	−.069	−.062	−.052	−.054	−.048	−.052	−.052	−.060
93.5	−.155	−.149	−.152	−.099	−.096	−.065	−.089	−.125	−.125	−.121	−.135	−.135	−.154
96.0	−.123	−.110	−.113	−.081	−.078	−.058	−.073	−.125	−.125	−.129	−.141	−.141	−.170

TABLE VIII.– PRESSURE-COEFFICIENT DATA PRESENTED IN FIGURES 16 AND 17 AT POSITION $\phi = 180^{\circ}$ ON THE TOP CANOPY

Station (percent)	Angle of attack (deg)						
	–5	0	2	4	6	8	10
1.8	0.338	0.248	0.212	0.186	0.163	0.142	0.122
5.1	.332	.244	.206	.178	.157	.138	.118
8.5	.475	.357	.308	.254	.205	.184	-----
10.9	.461	.363	.328	.297	.270	.243	.214
22.0	–.143	–.184	–.190	–.203	–.219	–.226	–.238
34.5	–.030	–.040	–.039	–.039	–.034	–.023	–.014
46.1	.014	.020	.001	–.001	–.002	–.001	–.006
60.0	–.010	–.020	–.027	–.021	–.016	–.013	–.012
73.0	–.002	–.006	–.013	–.019	–.008	–.001	–.004

NACA

TABLE IX.– SUPPLEMENTARY PRESSURE–COEFFICIENT DATA AT

POSITION $\phi = 180^{\circ}$ ON THE TOP CANOPY

Station (percent)	Angle of attack (deg)										
	–5	–3	–3	–2	–2	0	2	4	6	8	10
1.8	0.337	0.301	0.301	0.283	0.285	0.249	0.214	0.186	0.160	0.142	0.122
5.1	.331	.293	.293	.277	.277	.243	.208	.179	.154	.138	.120
8.5	.474	.426	.426	.405	.405	.357	.311	.254	.200	.184	-----
10.9	.462	.421	.423	.403	.405	.365	.329	.298	.268	.243	.214
22.0	–.143	–.162	–.163	–.168	–.169	–.183	–.187	–.202	–.221	–.226	–.236
34.5	–.030	–.038	–.035	–.038	–.037	–.041	–.037	–.038	–.035	–.023	–.012
46.1	.016	.006	.006	.014	.013	.019	.002	0	–.005	–.001	–.004
60.0	–.010	–.018	–.015	–.018	–.019	–.021	–.025	–.020	–.019	–.011	–.010
73.0	0	–.006	–.003	–.008	–.007	–.007	–.011	–.012	–.011	–.001	–.004

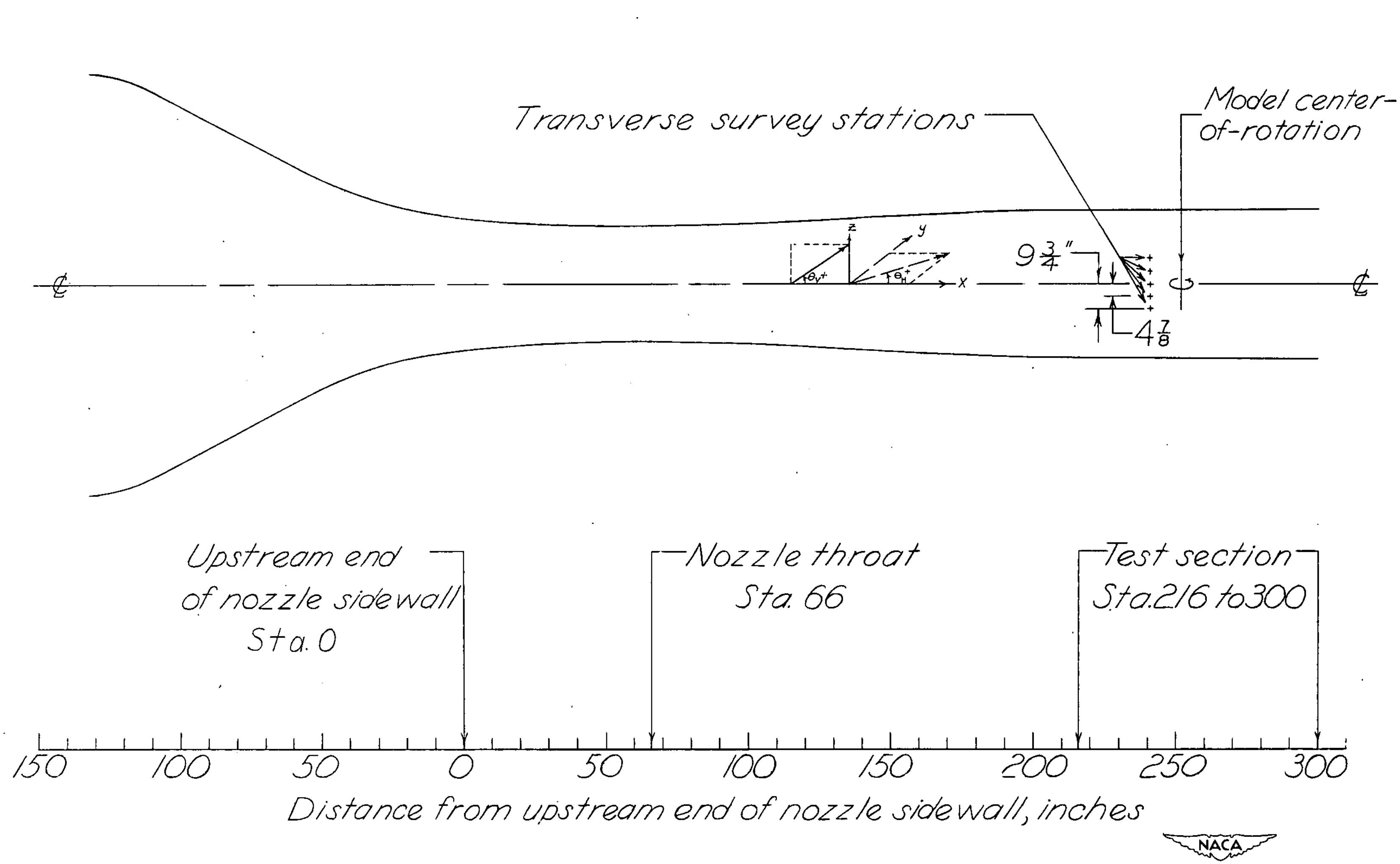

Figure 1.- Schematic layout of entrance cone, nozzle, and test section of the Langley 4- by 4-foot supersonic tunnel.

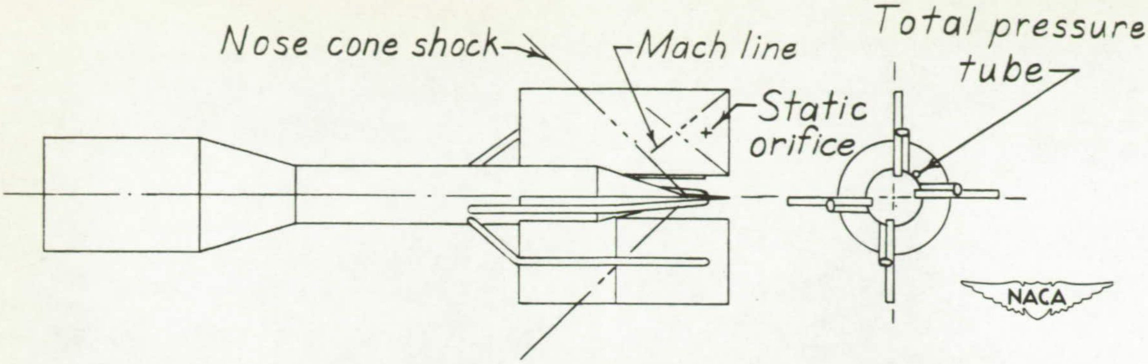

(a) Schematic drawing of cruciform probe.

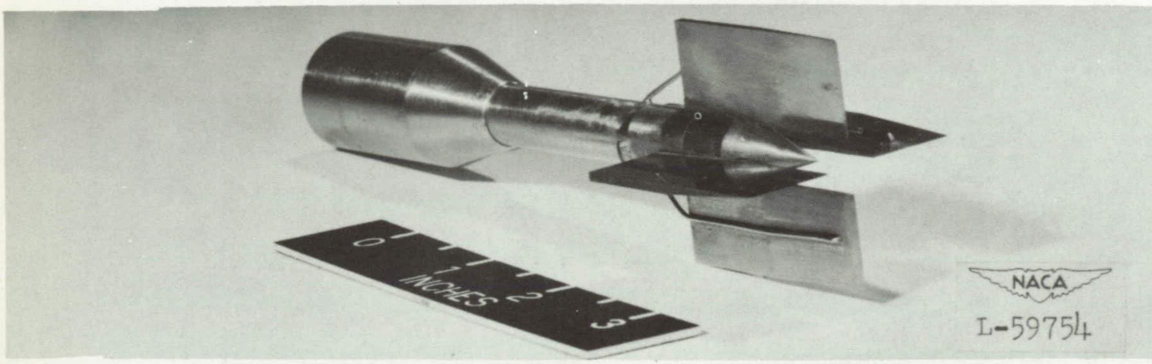

(b) Three-quarter-front view of cruciform probe.

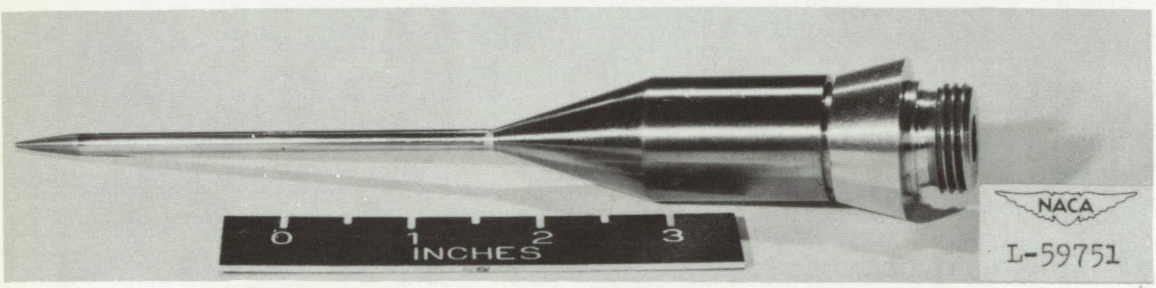

(c) Pitot-static probe.

Figure 2.- Calibration probes.

Page intentionally left blank

Page intentionally left blank

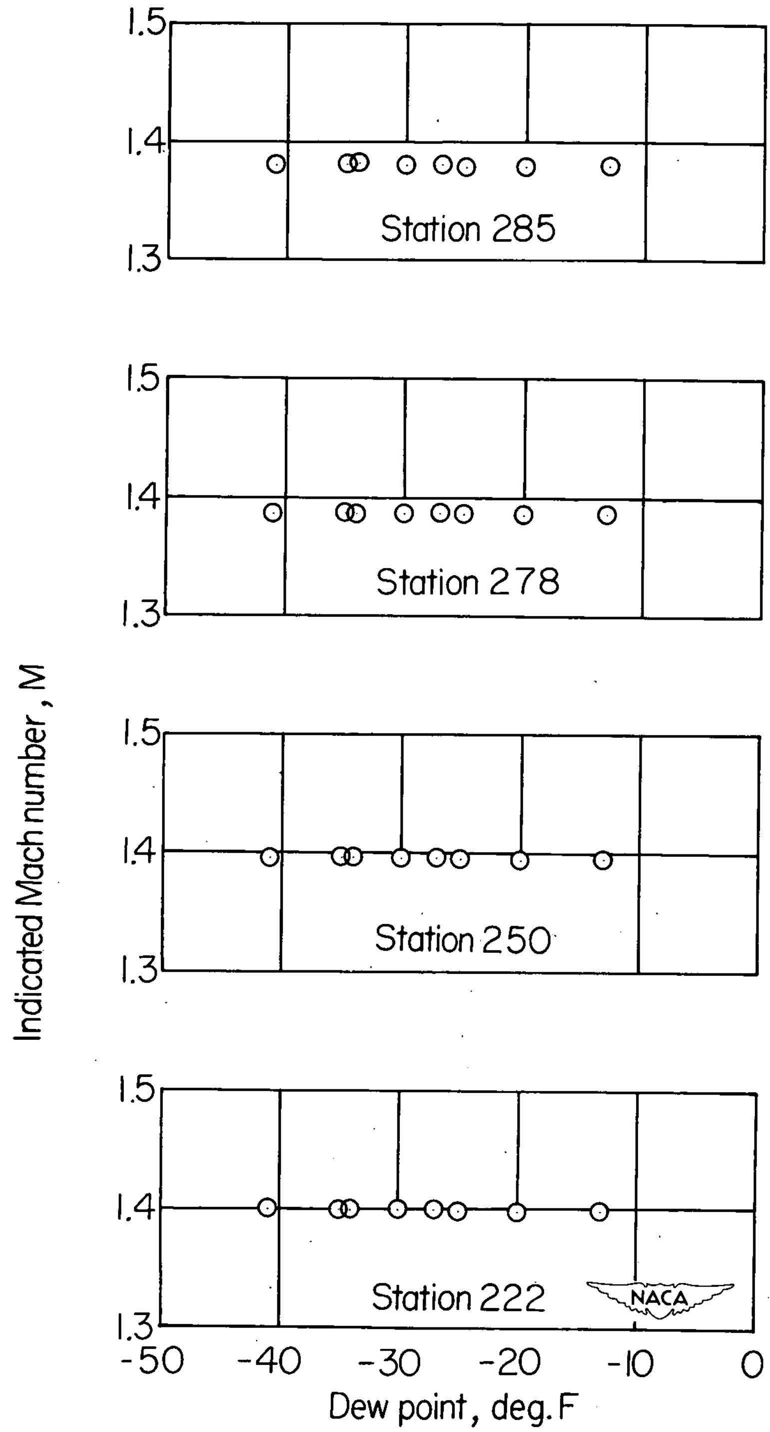

Figure 3.- Variation of local Mach number with dew point for representative upper-wall stations along nozzle axis of the Langley 4- by 4-foot supersonic tunnel for a stagnation temperature of 110° F and 0.25-atmosphere stagnation pressure.

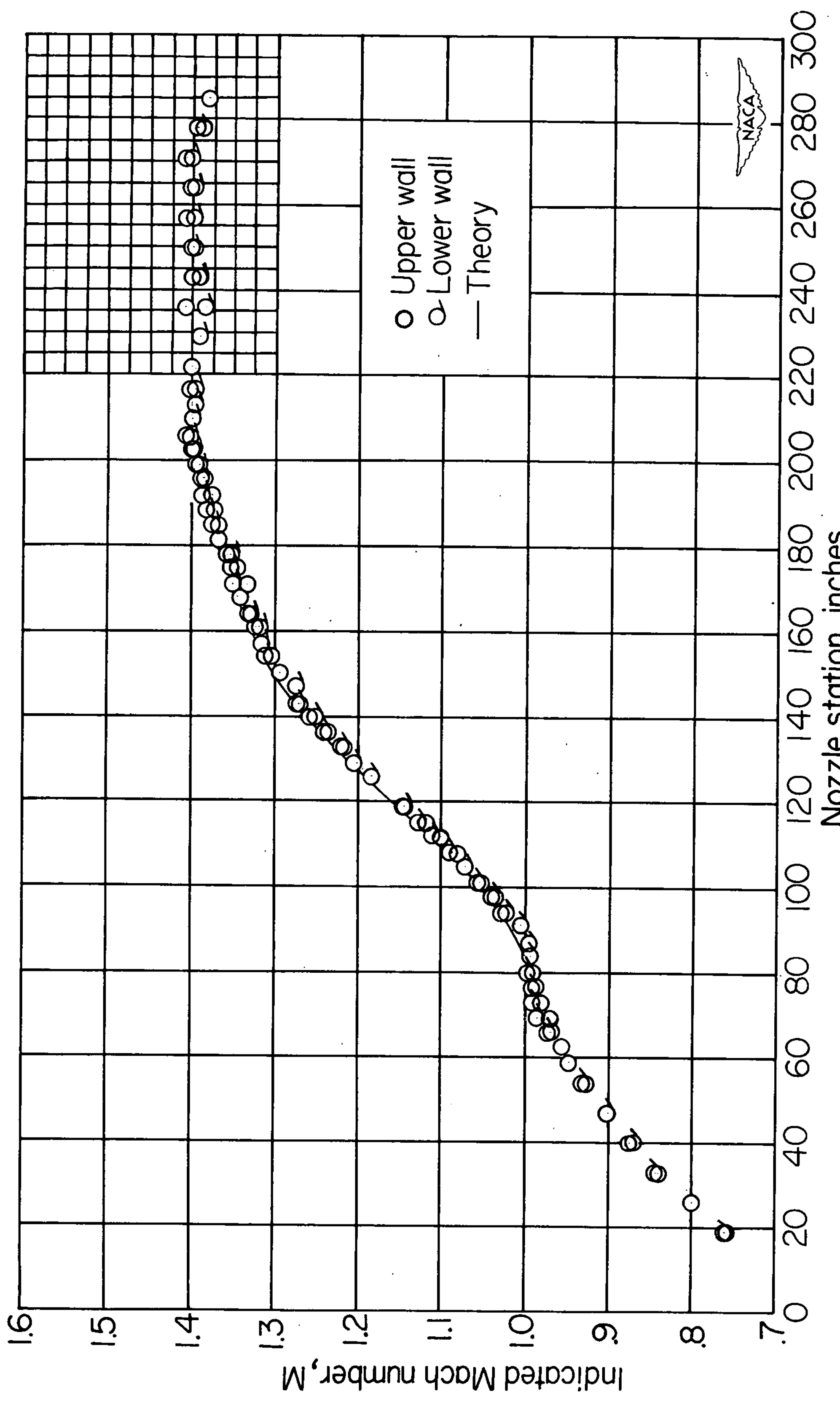

Figure 4.- Mach number distribution along center line of nozzle walls of the Langley 4- by 4-foot supersonic tunnel.

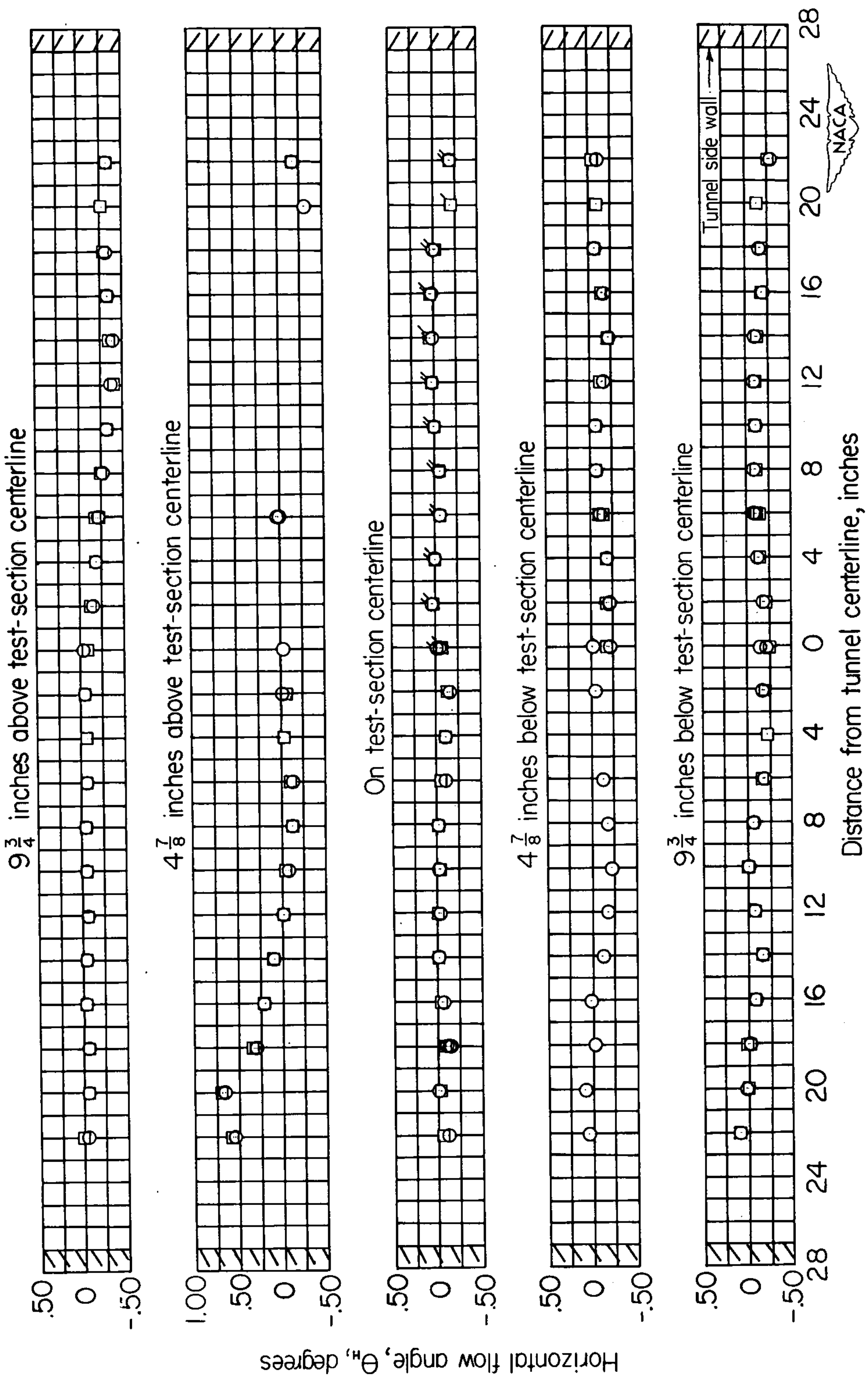

(a) Horizontal flow angle, θ_H, degrees.

Figure 5.- Stream conditions in a transverse plane looking upstream at station 241 in test section of M = 1.40 nozzle of the Langley 4- by 4-foot supersonic tunnel.

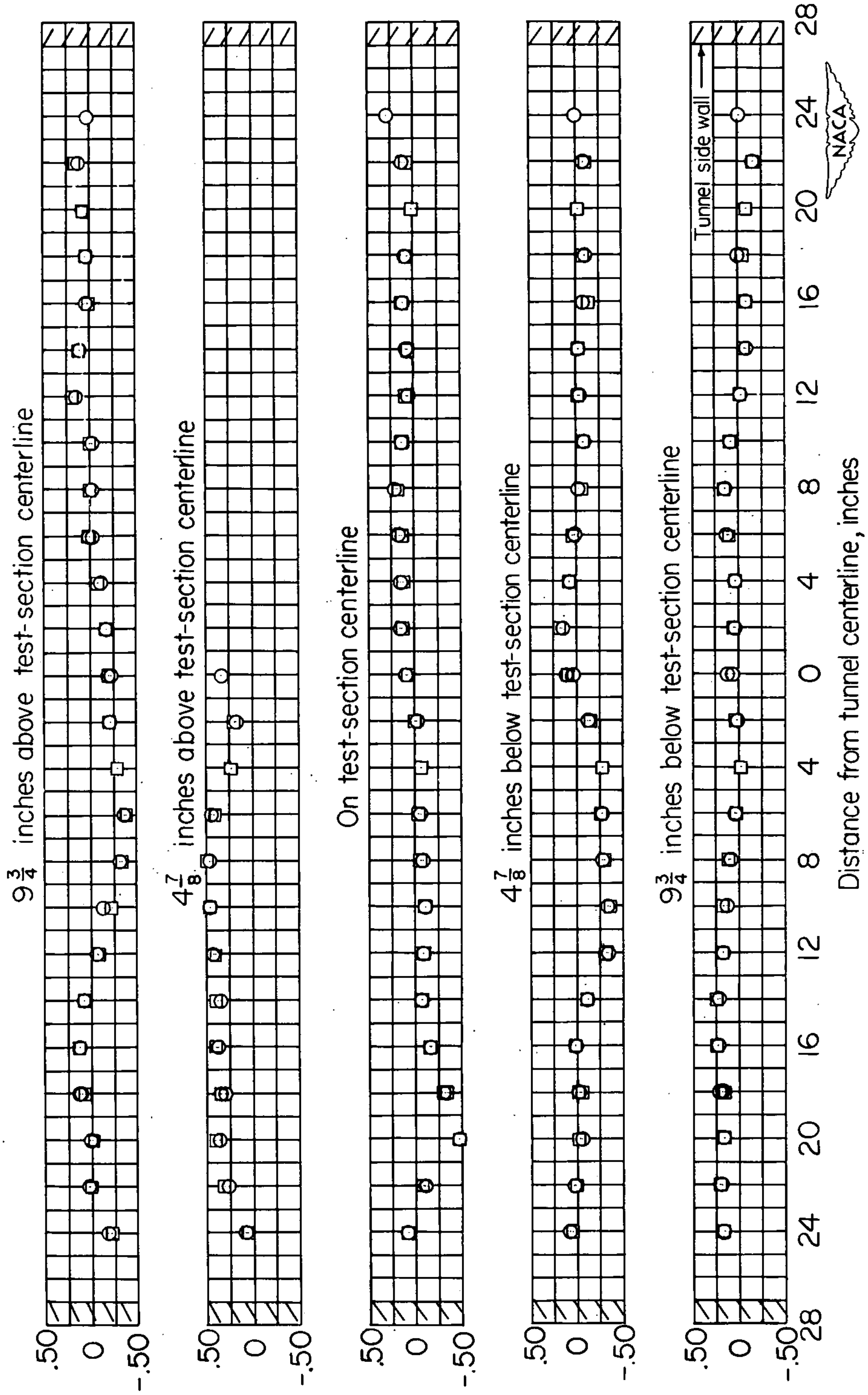

(b) Vertical flow angle, θ_V, degrees.

Figure 5.- Continued.

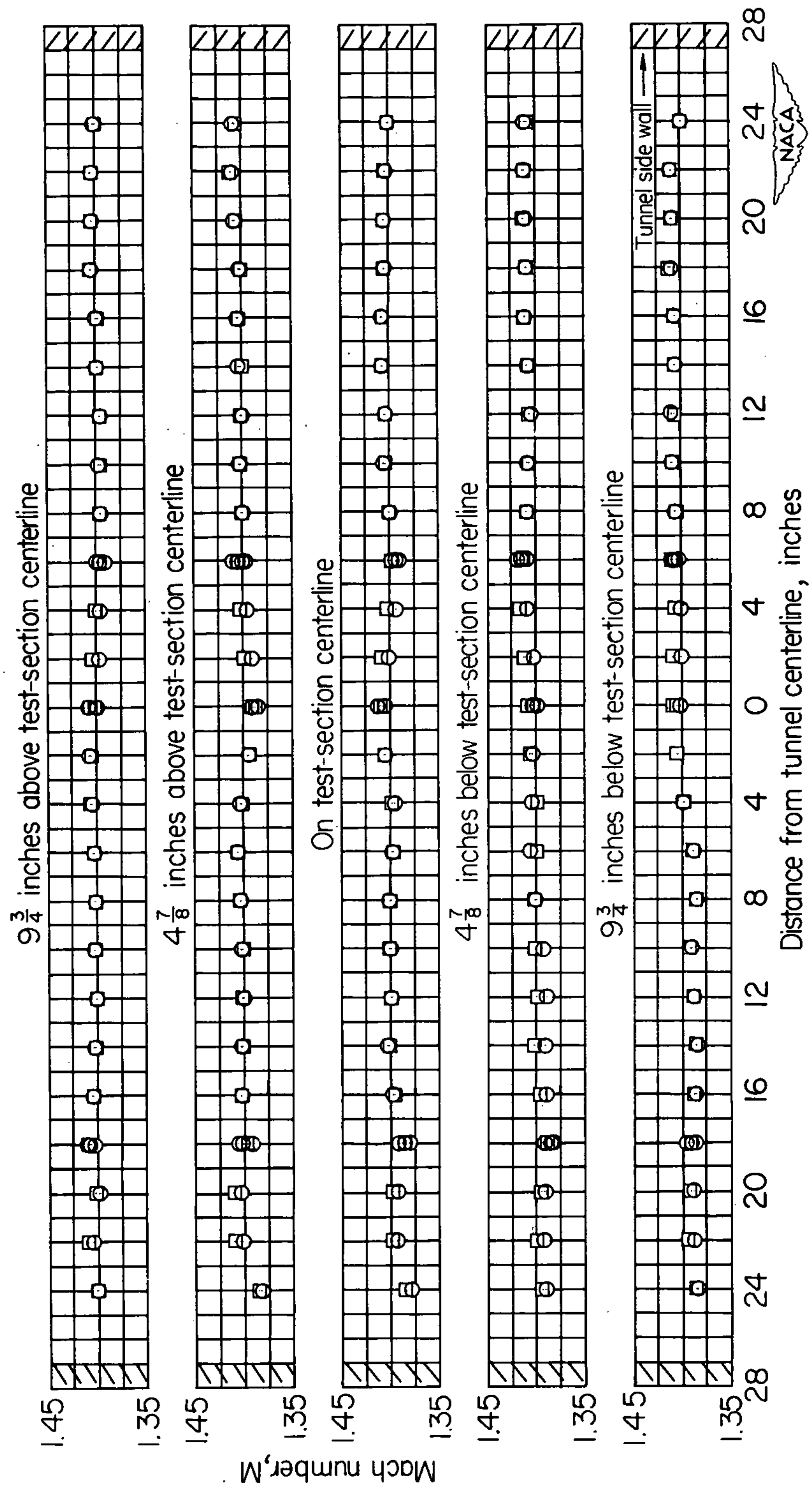

(c) Mach number.

Figure 5.- Concluded.

Page intentionally left blank

Page intentionally left blank

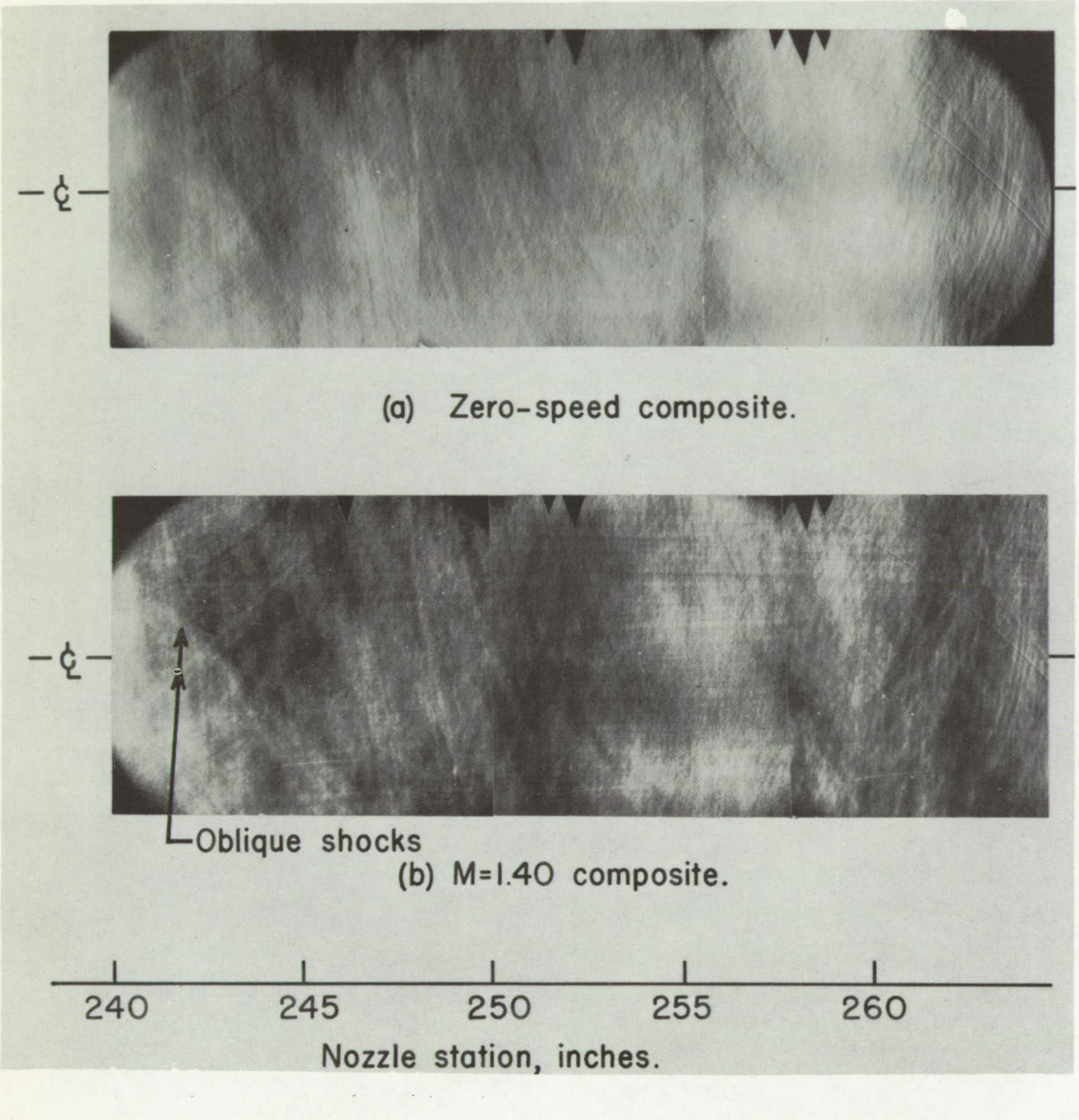

Figure 6.- Schlieren photographs of flow on test section center line of M = 1.40 nozzle.

Page intentionally left blank

Page intentionally left blank

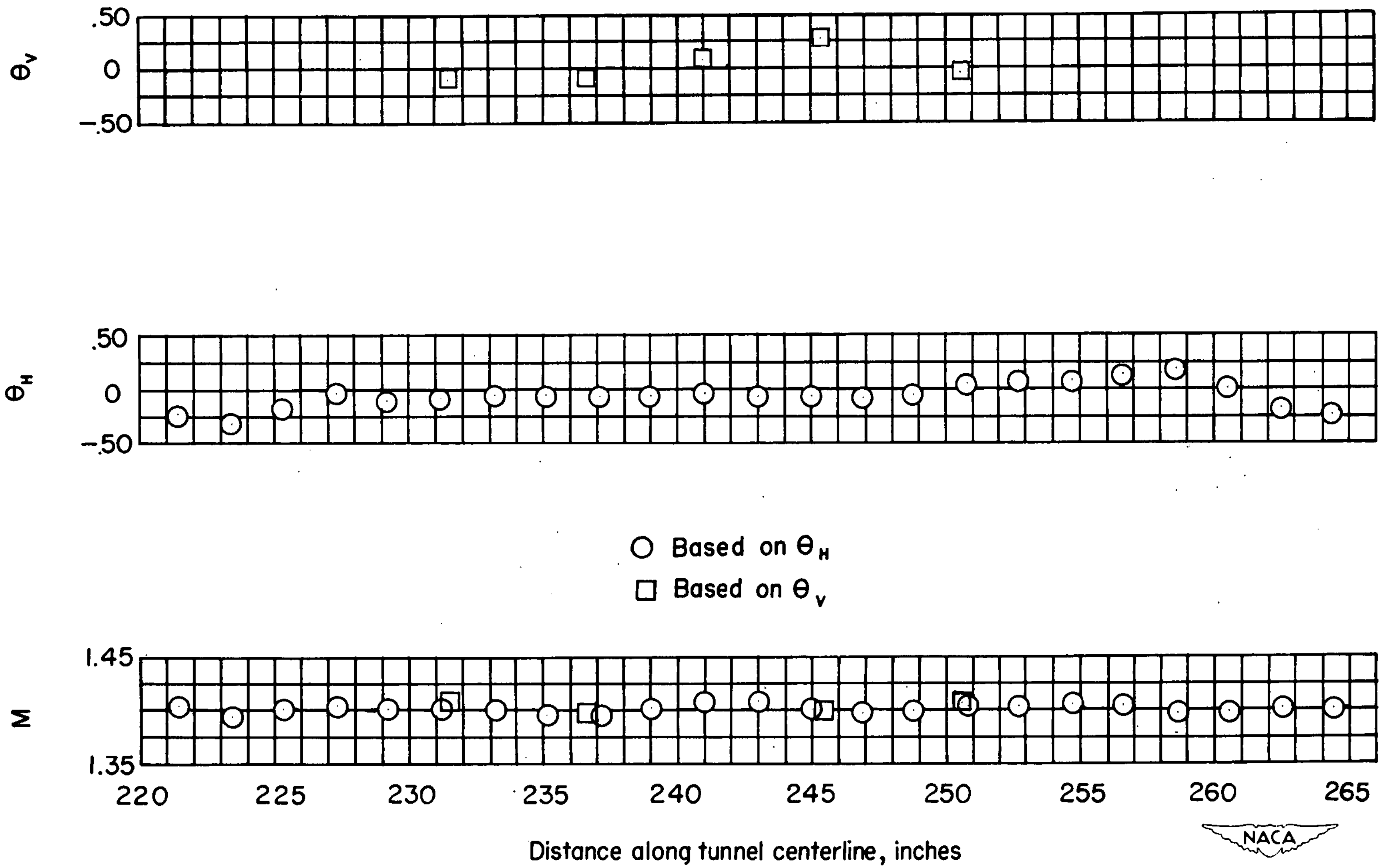

Figure 7.- Variation of Mach number and flow angle along center line of M = 1.40 nozzle of the Langley 4- by 4-foot supersonic tunnel.

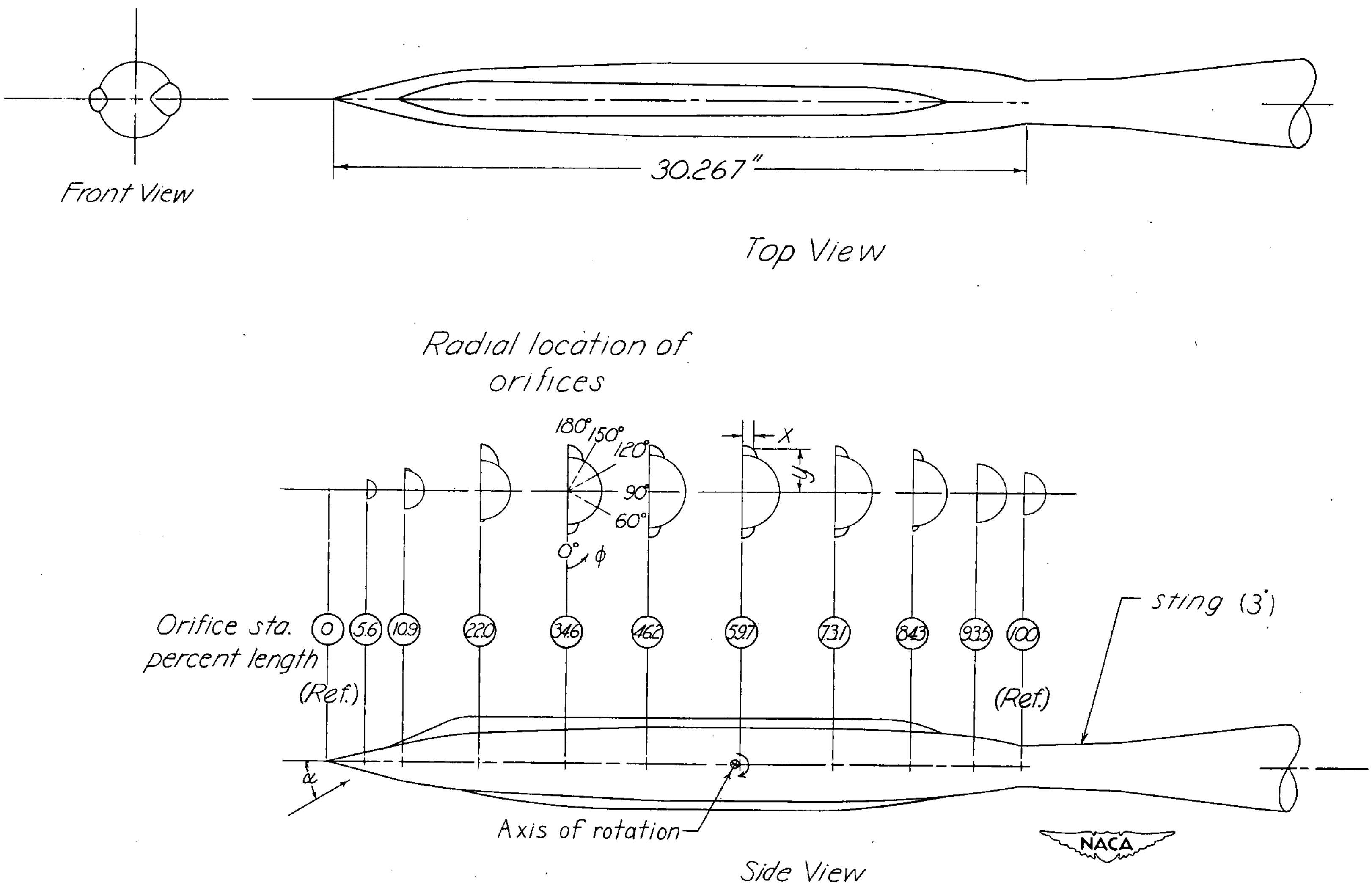

Figure 8.- Fuselage model layout. Coordinates are given in table I.

Figure 9.- Downstream view of the body of revolution in the Langley 4- by 4-foot supersonic tunnel.

Page intentionally left blank

Page intentionally left blank

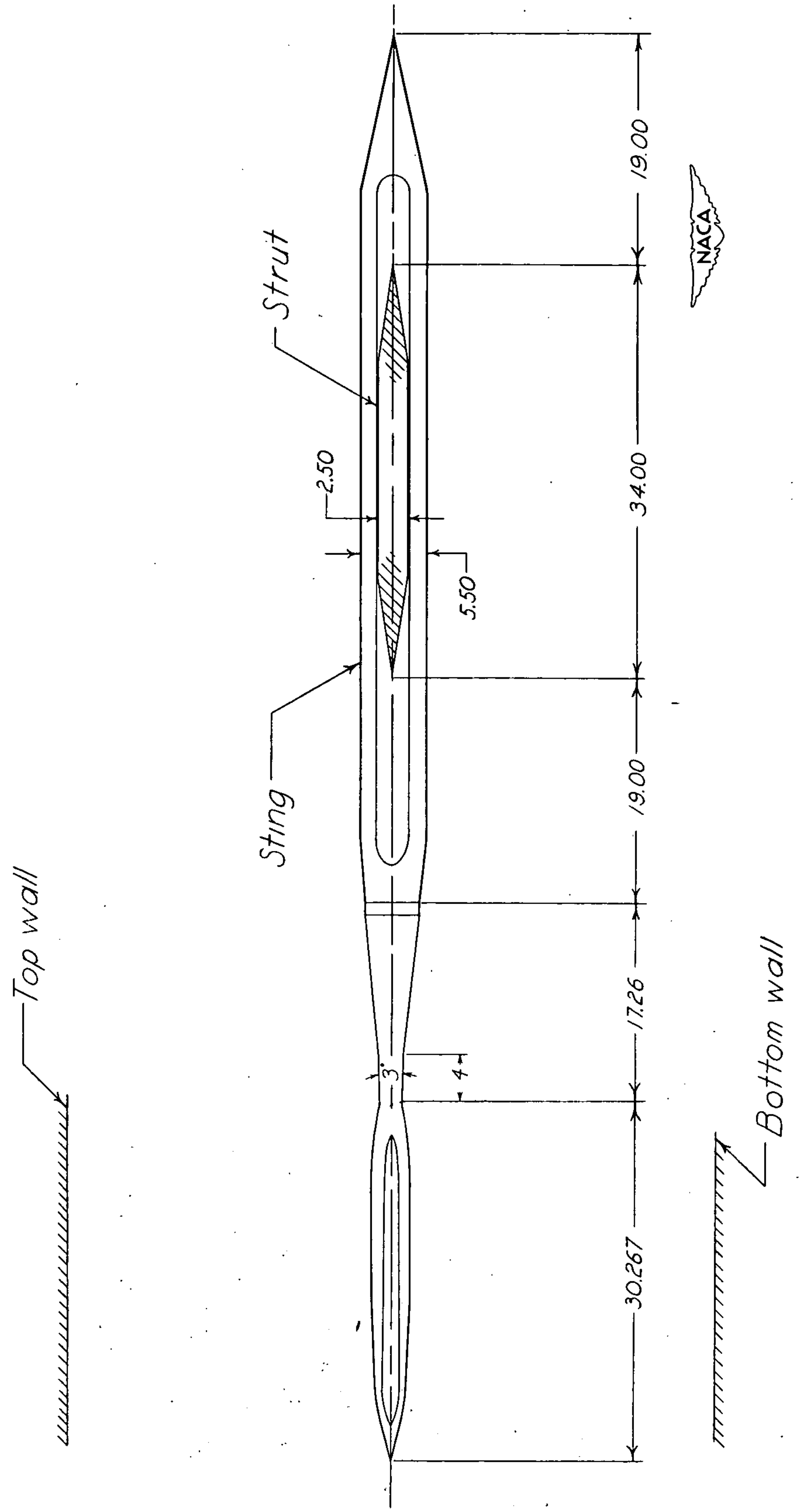

Figure 10.- Model and support installation. All dimensions are in inches.

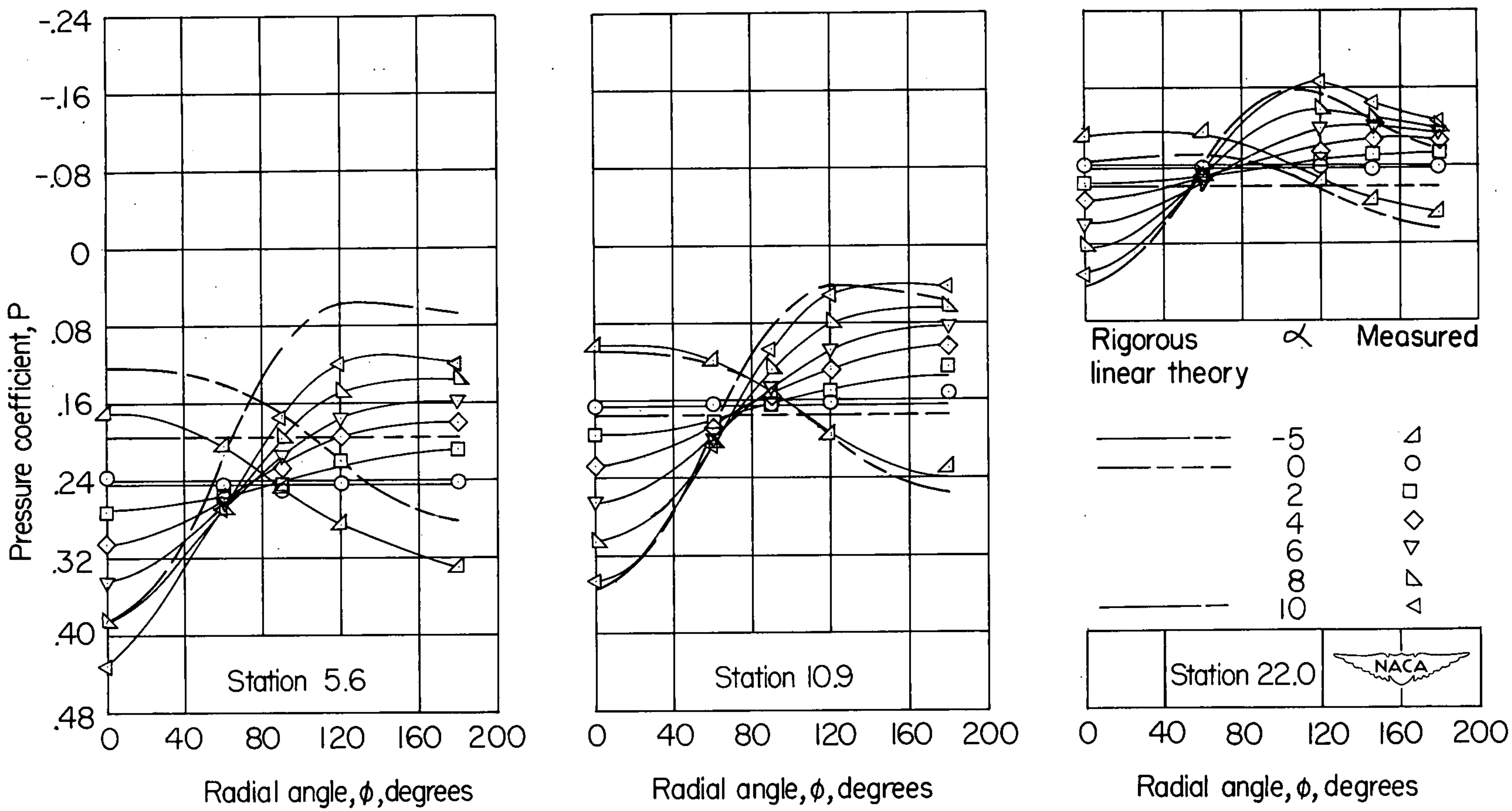

Figure 11.- Variation of pressure coefficient with radial location at nine axial stations on the body of revolution at $M = 1.40$.

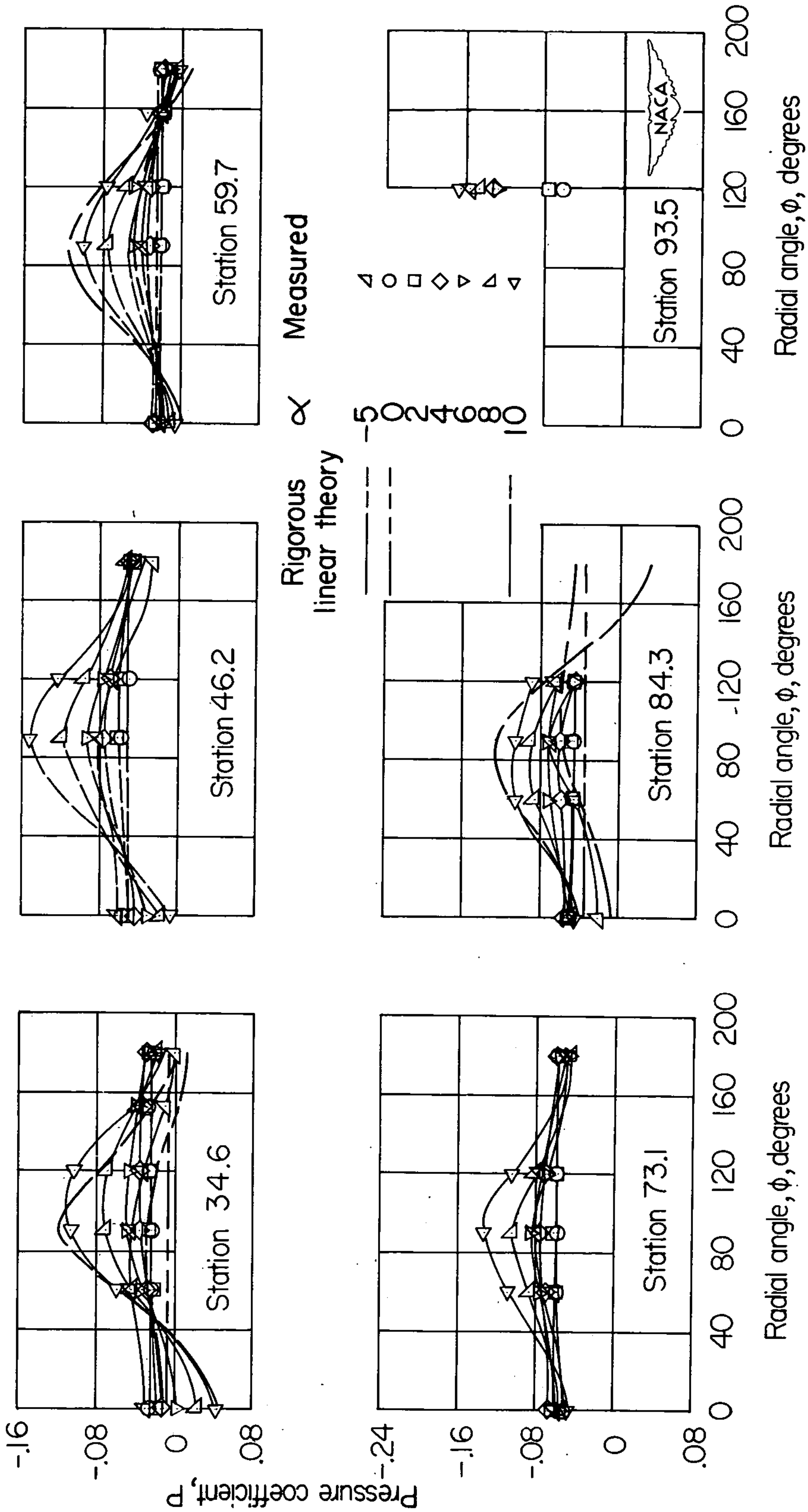

Figure 11.- Concluded.

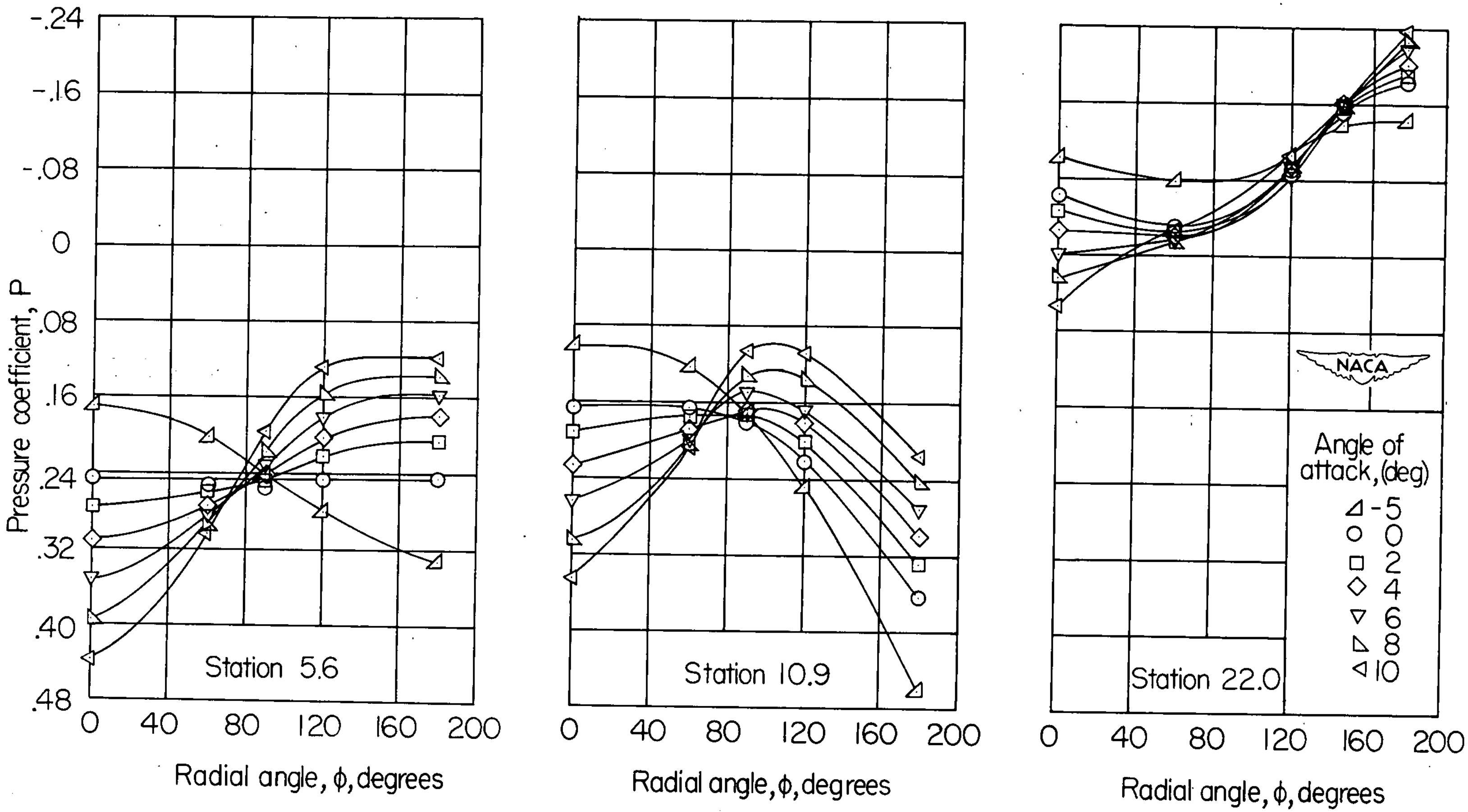

Figure 12.- Variation of pressure coefficient with radial location at nine axial stations on the fuselage with canopies, M = 1.40.

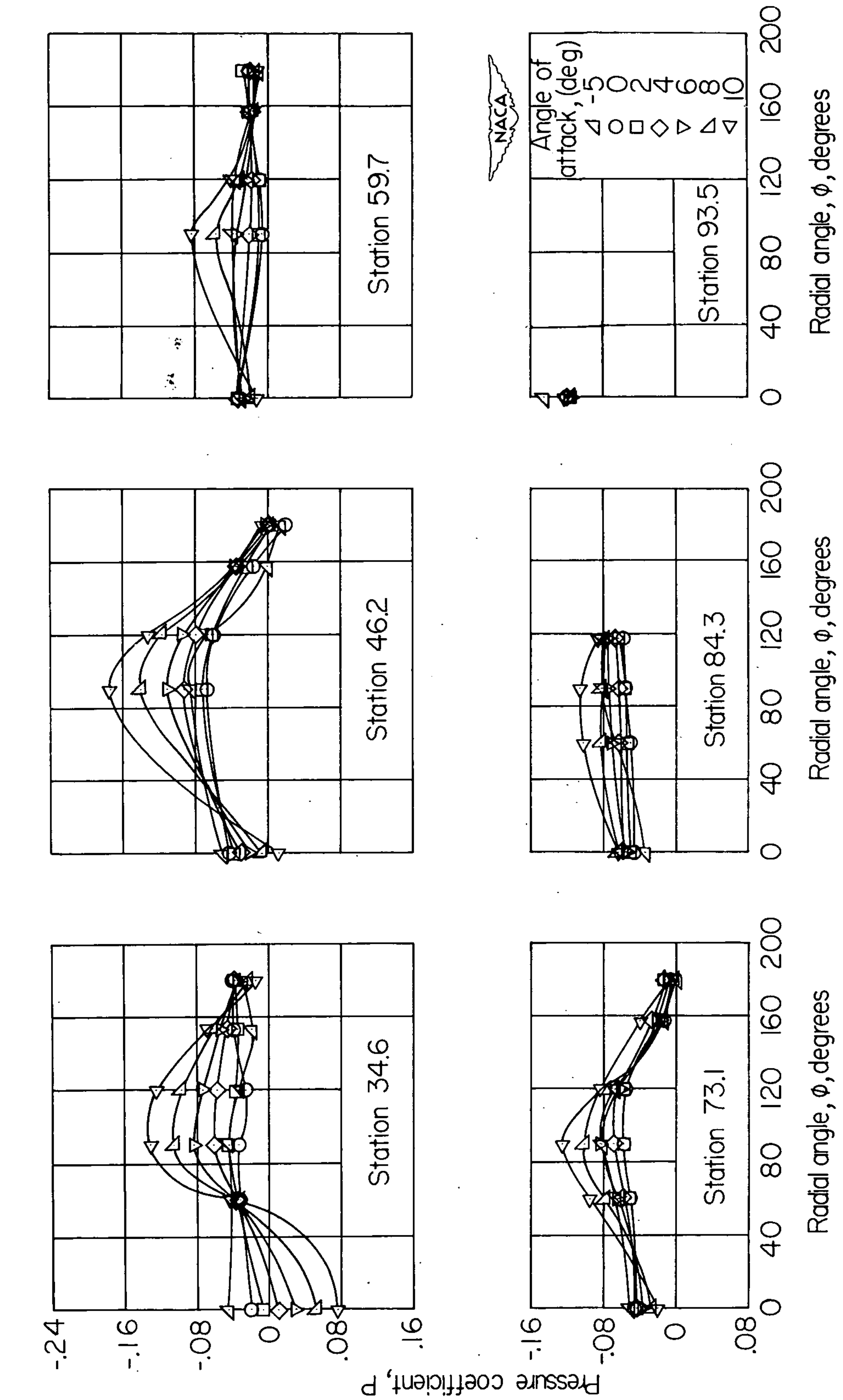

Figure 12.- Concluded.

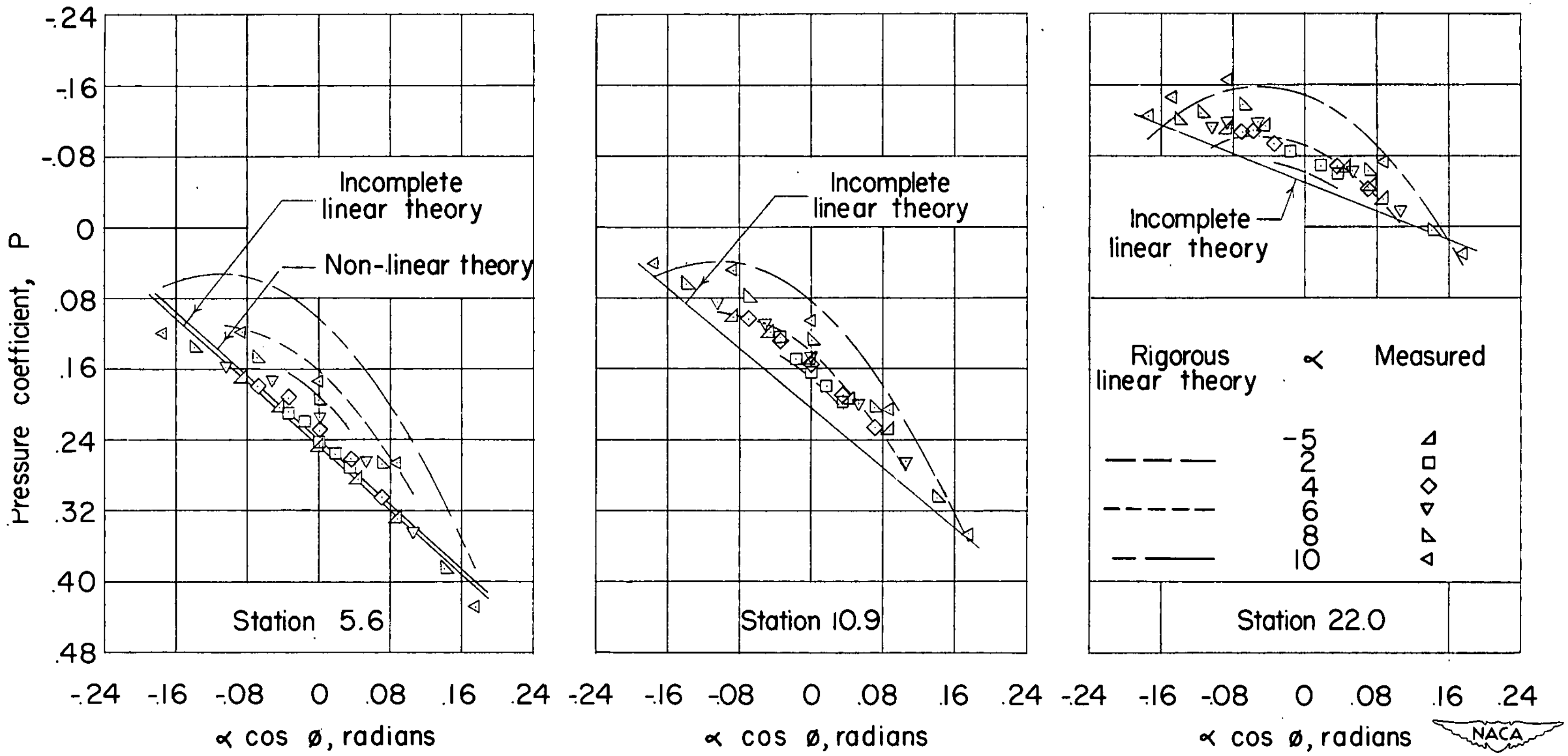

Figure 13.- A comparison of the theoretical and experimental pressure-coefficient variation with $\alpha \cos \phi$ at nine axial stations on the body of revolution, M = 1.40.

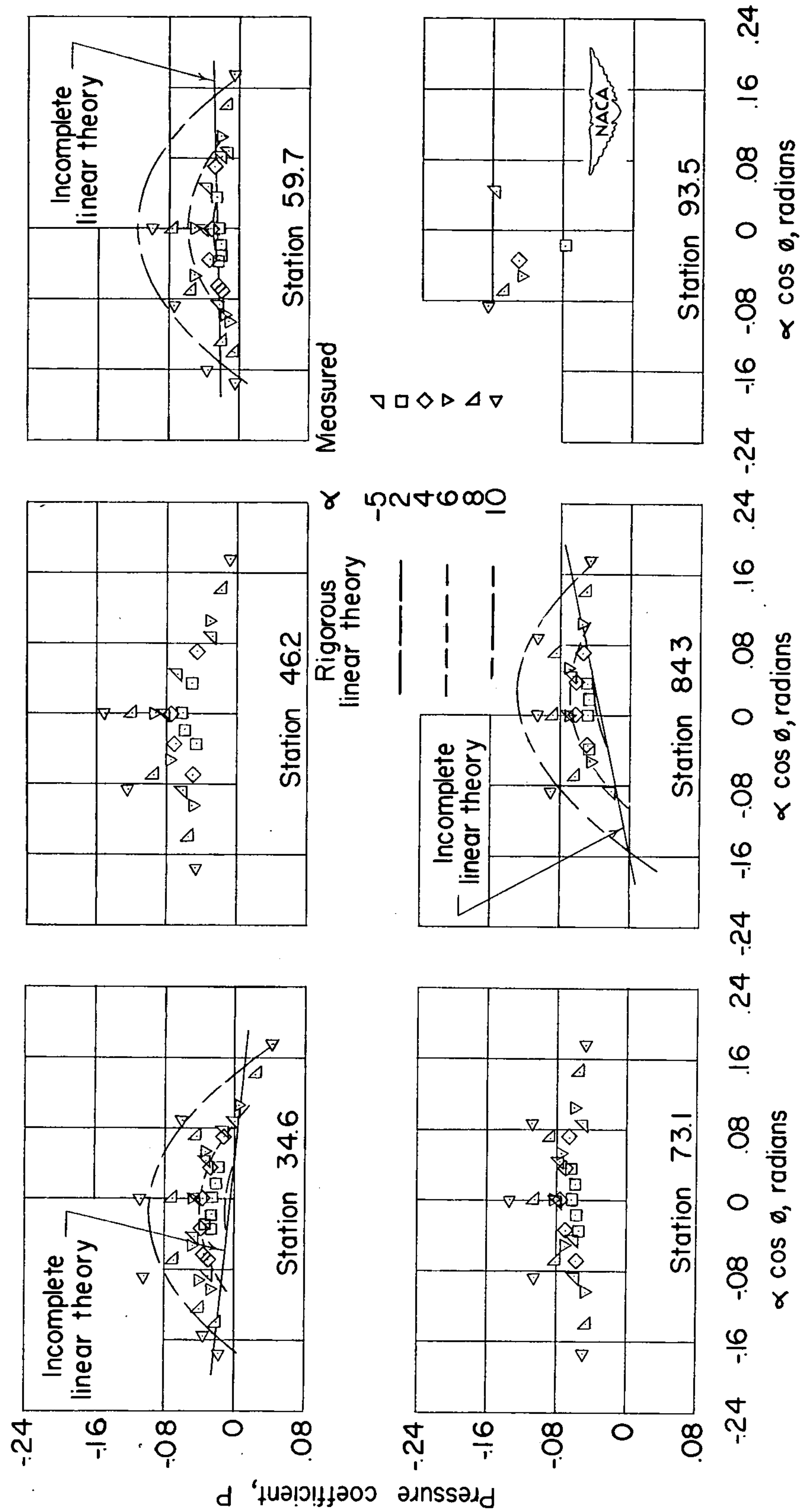

Figure 13.- Concluded.

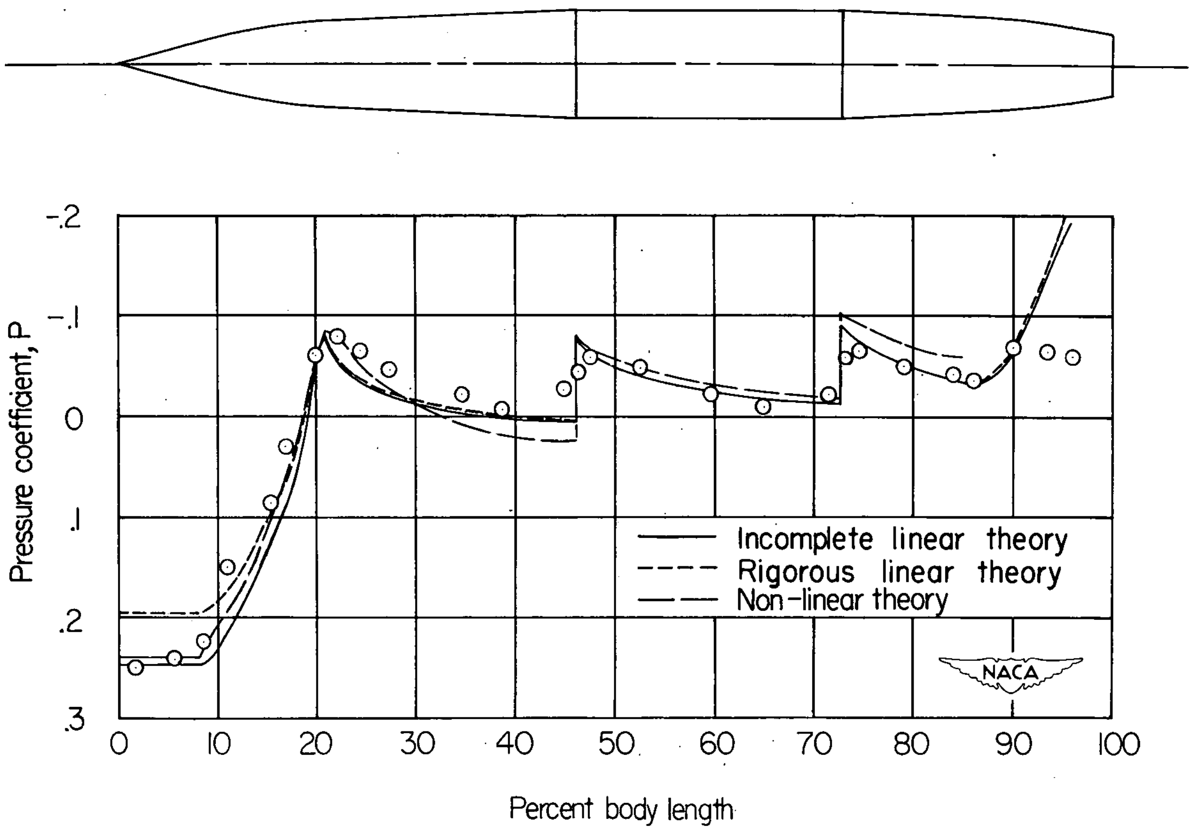

Figure 14.- A comparison of the theoretical and experimental axial pressure distribution at 0° angle of attack along the top surface ($\phi = 180^{\circ}$) of the body of revolution, M = 1.40.

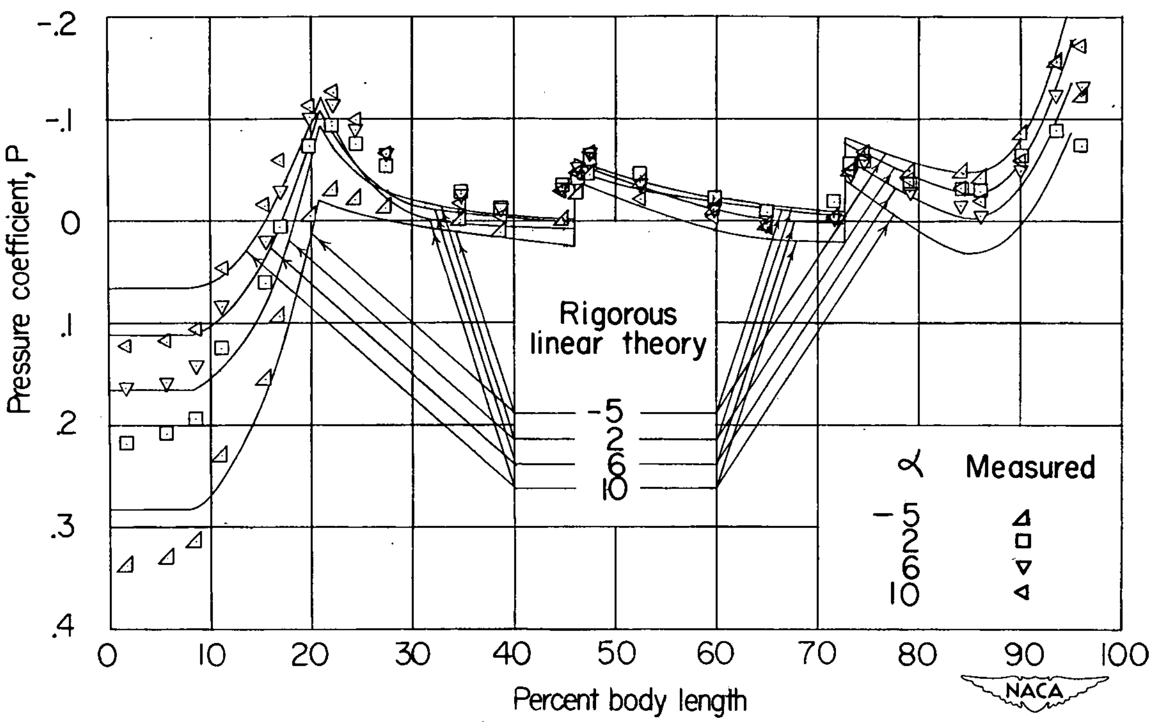

Figure 15.- A comparison of the theoretical and experimental axial pressure distribution at several angles of attack along the top surface (ϕ = 180°) of the body of revolution, M = 1.40.

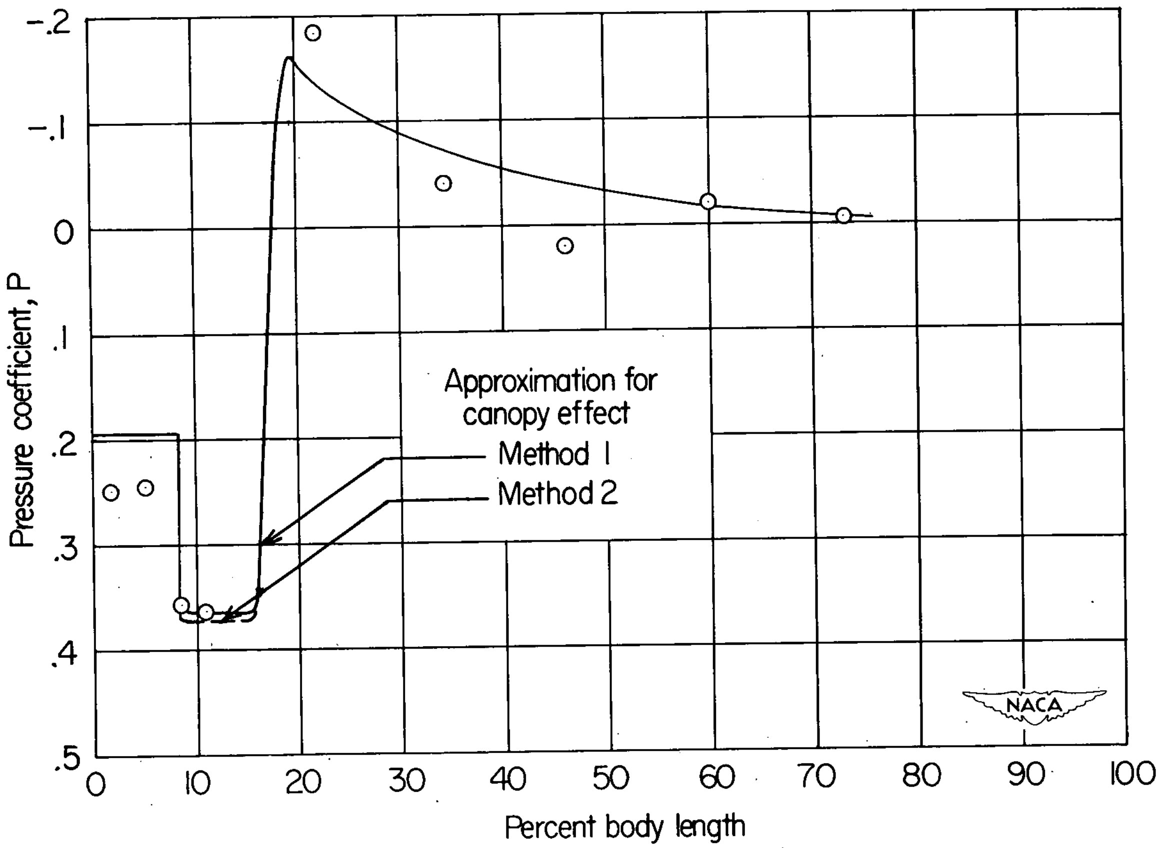

Figure 16.- A comparison of the experimental and estimated pressure distribution at 0° angle of attack on the top fuselage canopy (ϕ = 180°), M = 1.40.

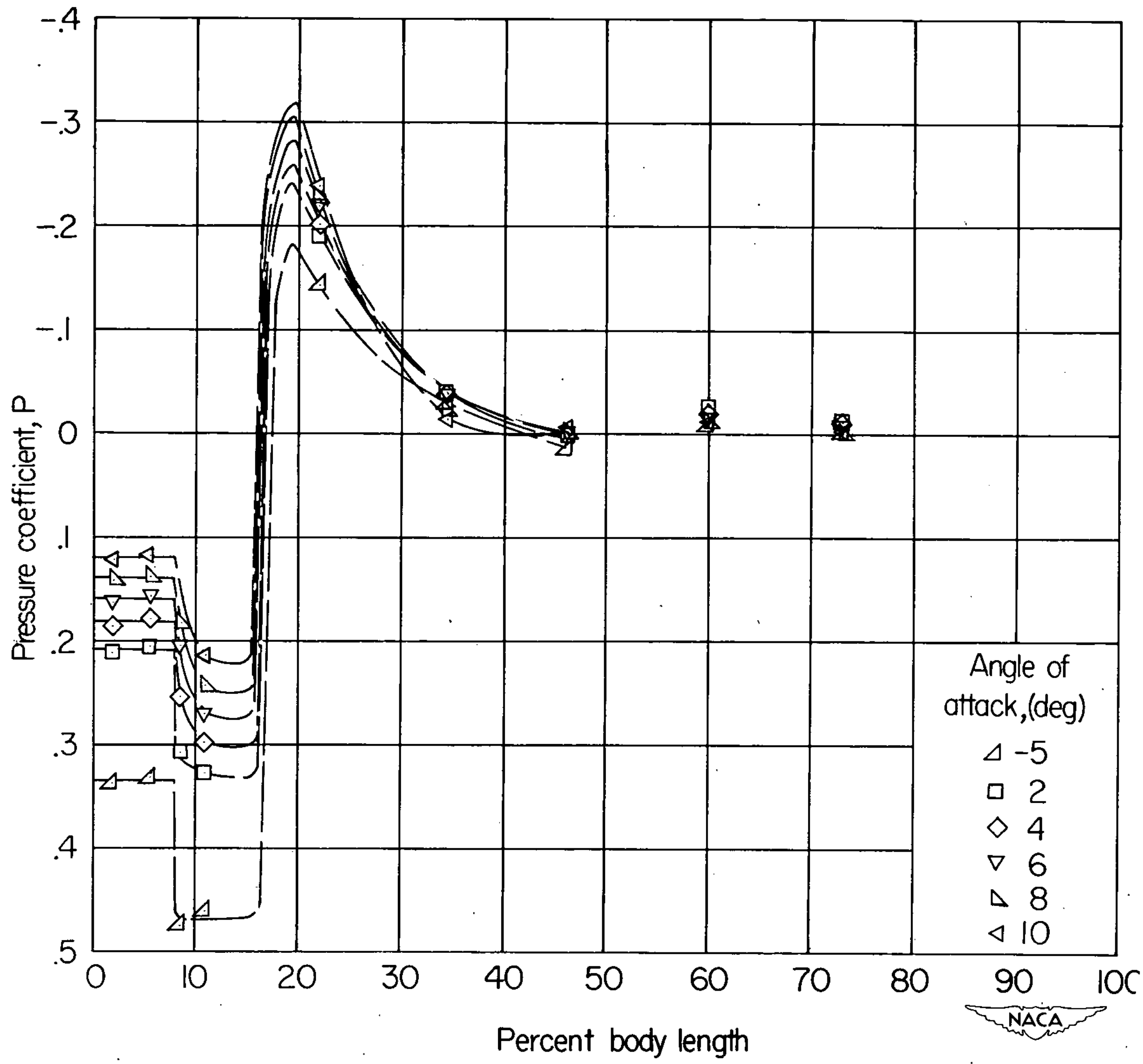

Figure 17.- The experimental pressure distribution at several angles of attack on the top surface (ϕ = 180°) of the fuselage canopy, M = 1.40.